Incorporation of Nitrogen and Nano-diamonds into Diamond-Like Carbon Coatings on Ti-6Al-4V for Enhancement of Wear and Corrosion Resistance

A thesis submitted to the College of

Graduate Studies and Research

In Partial Fulfillment of the requirements

For the Degree of Master of Science

In the Department of

Mechanical Engineering

University of Saskatchewan

Saskatoon

By

Santu Bhattacherjee

PERMISSION TO USE

In presenting this thesis in partial fulfillment of the requirements for a postgraduate degree from University of Saskatchewan, I agree that libraries of this university may make it freely available for inspection. I further agree that permission for copying of this thesis in any manner, in whole or in part, for scholarly purposes may be granted by the professor Dr Qiaoqin Yang who supervised my thesis work or, in her absence, by the Head of the Department or the Dean of the college in which my thesis work was done. It is understood that any copying or publication or use of this thesis or parts thereof for financial gain shall not be allowed without my written permission. It is also understood that due recognition shall be given to me and to University of Saskatchewan in any scholarly use which may be made of any material in my thesis.

Requests for permission to copy or to make other use of material in this thesis in whole or part should be addressed to:

Head of the Department of Mechanical Engineering
57 Campus Drive, Saskatoon, SK
University of Saskatchewan
Saskatoon, Saskatchewan S7N 5A9
Canada

ABSTRACT

Titanium and its alloys are widely used for industrial applications. However, extended use of titanium in some applications has been severely limited due to its poor surface properties. Diamond-like carbon (DLC), which is a special group of amorphous carbon materials, can be highly beneficial in this regard. In the past decades, nitrogen incorporation into DLC has gained significant attention due to enhanced quality in terms of stress reduction, electrochemical and mechanical properties. However, so far the reports on the chemical structure of nitrogen-doped DLC have not been conclusive as nitrogen tends to form different bonding configuration with carbon depending on deposition methods.

In the present thesis, a low energy End-Hall ion beam source (E-H source) was used to deposit nitrogen-incorporated DLC thin films on Ti-6Al-4V sheets. The adhesion, mechanical and electrochemical properties of DLC and nitrogen- incorporated DLC (N-DLC) were investigated. In order to improve interfacial adhesion, Ti-6Al-4V sheets were first treated in a microwave plasma enhanced chemical vapour deposition (MPCVD) reactor to grow nanodiamond particles on their surface. DLC and N-DLC coatings were then deposited on them by ion beam deposition. Silicon wafers were also used as the substrate for reference. Raman spectroscopy, X-ray absorption spectroscopy (XAS), X-ray photoelectron spectroscopy (XPS), scanning electron microscopy (SEM), and optical profilometry were used to characterize the chemical and morphological structure of the coatings. Nanoindentation and Rockwell C testing were used for measuring the mechanical and adhesion properties, respectively. DLC showed a hardness value of 11 GPa, whereas N-DLC showed slightly lower hardness because of the increased graphitic bonding, demonstrated by Raman and XPS results. The optical profilometer measurements shows a decrease in surface roughness with nitrogen doping while Rockwell C testing shows that the nanodiamond particles grown on titanium alloy surface greatly enhance the adhesion of DLC and a small amount of nitrogen doping further improves the adhesion.

N-DLC coated samples showed reduced coefficient of friction (COF) when measured against UMPHE balls. The COF showed monotonic decrease with increase in nitrogen concentration. Significant reduction in the wear rates were observed for N-DLC against SS 440C steel balls. The samples with N/C ratio of 0.27 show the lowest wear rate. The corrosion resistance was evaluated by Tafel polarization and Electrochemical Impedance Spectroscopy. N-DLC with pre-deposited nanodiamonds on titanium substrate alloys showed significant improvement in corrosion resistance compared to bare titanium alloy substrate in 0.89% NaCl solution.

ACKNOWLEDGEMENTS

I am highly grateful to Dr Qiaoqin Yang for providing me an excellent opportunity to carry out my research in University of Saskatchewan and supervising and guiding me throughout my research project. I would also like to extend my thanks to Dr Jerzy Spzunar and Dr Ike Oguocha for their valuable advice. The training and assistance provided by Mr. Zhao Nan Fang, Mr. Robert Peace and Mr. Jason Maley were highly helpful for the experiments carried out in this work.

I would also like to acknowledge the contributions of my colleagues, Ms. Parisa Ashtijoo and Dr. Haidong Wang for their constructive contributions to the work.

This research was funded by Canada Research Chair program, Natural Sciences and Engineering Research Council (NSERC), Canada, Canada Foundation for Innovation (CFI), and University of Saskatchewan.

DEDICATION

This work is dedicated to my family members, friends

and

to my loving parents Chandan Bhattacherjee and Tapasi Bhattacherjee

Table of Contents

LIST OF FIGURES:

LIST OF TABLES:

Chapter 1
Introduction

1.1. Motivation

Titanium has found broad industrial applications such as aerospace, biomedical, chemical, and marine (Boyer, 1996; Budinski, 1991; Rack & Qazi, 2006; Yamada, 1996) because of its high specific strength, high toughness, good biocompatibility, and relatively high corrosion resistance to other common metals. However, extended applications of titanium alloys are severely limited in most cases due to its poor tribological performance and long term corrosion failure (Agins et al., 1988; Budinski, 1991). Diamond-like carbon (DLC) is an amorphous carbon with high amount of sp^3 bonding renowned for its unique qualities such as high hardness, high corrosion resistance, low friction coefficient, optical transparency, and excellent biocompatibility. Thus it can be served as a protective coating to enhance the surface properties of titanium alloy for their engineering applications (Erdemir & Donnet, 2006; Grill, 1993).

However, DLC coatings normally have high residual stress due to its synthesis method that requires the bombardment of high energetic ions (Robertson 2002). High residual stress in DLC causes poor adhesion to Ti alloys and most of the other metallic substrates (Grill 1993; Robertson 2002; Zhang et al. 2013). Research in the past had adopted various techniques to minimize the stress in DLC to improve its adhesion to the substrates. Those include using a single buffer interlayer (Si,Cr) (Costa et al. 2011; Kim et al. 2005), functionally graded interlayers (Ti/TiC/DLC, Ti/TiN/DLC, Ti/TiN/TiNC/DLC) (Choy & Felix, 2000), surface pretreatment of the substrates by Ar plasma, doping with various metallic (Ti, Cr, Ni) and non - metallic elements (N, F, Br, B) (Anita et al. 2004; Singh et al. 2006). Functionally graded interlayers were able to effectively improve adhesion between DLC and substrates, nevertheless, complicated procedures are needed. It is very challenging to control the interfacial property of such multilayers as poor interface can cause catastrophic failure of DLC. Thus, simple techniques which can enhance coating adhesion to the substrate are highly desirable.

Recent studies showed a significant increase in adhesion of DLC thin films on Ti alloys by incorporation of nanodiamonds (Zhang et al. 2013) and a decrease in residual internal stress by doping of DLC with elements like nitrogen (Dwivedi et al. 2011). It is expected that incorporation of both nanodiamonds and nitrogen would greatly enhance the lifespan of DLC coatings by increasing adhesion and minimizing stress-related failures. Hence, nanodiamond and nitrogen incorporated DLC thin films would be promising to serve as a protective coating onto Ti alloys for improving its surface properties. However, the properties of such composite coatings have not been fully investigated as required for practical applications. Systematic studies on thosecoatings are necessary in order to have more in-depth understanding of those composite coatings for application development.

1.2. Objectives

The overall goal of the present research is to improve the tribological and corrosion resistant properties of Ti-6Al-4V for wider applications. The specific objectives of the present research are:

1. To enhance the adhesion of carbon coatings by deposition of nanodiamond particles on titanium alloys by MPCVD system.
2. To synthesize of N-DLC thin films with different concentrations of nitrogen on nano-diamond predeposited Ti alloys using EH ion beam deposition.
3. To characterize the chemical bonding and microstructure to study the effect of doping in the coatings.
4. To evaluate the mechanical, electrochemical, and tribological properties of the films in an attempt to study the correlation of coating properties with regards to its chemical structure.

1.3. Thesis Organization

The present thesis comprises of five chapters. Chapter 1 focuses on research motivation, objectives of the present work and a brief outline of the thesis organization. Chapter 2 provides a detailed review of the structure, properties, deposition techniques, doping, growth mechanisms of DLC thin films and problems with DLC deposition. Chapter 3 describes the experimental details regarding deposition, corrosion tests, tribological and characterization of the thin films. Chapter 4 is divided into two sections and includes results and discussion about the bonding structure, surface roughness, adhesion, corrosion resistance and tribological properties of the films. Finally, conclusions and recommendation for future work is provided in Chapter 5.

Chapter 2

Literature Review

2.1 Carbon Materials and their Structures

Carbon has an atomic number of six. It has four valence electrons which can form covalent bonds either with other carbon atoms or atoms of different elements. Depending on different bonding configurations: sp^3, sp^2, sp^1, carbon forms a wide spectrum of materials which are both amorphous and crystalline. Figure 2.1 represents different bonding configurations of carbon. Carbon in its sp^3 configuration uses all four of its valence electrons to form strong σ bonds with adjacent atoms. The bonds in this case are tetrahedrally directed and this type of configuration is commonly seen in diamond, which is an allotrope of carbon. Three fold coordinated sp^2 is mostly found in graphite which is another allotrope of carbon. In sp^2 configuration three of the four valence electrons in carbon enter into trigonally directed σ bond in a plane. The fourth electron in sp^2 atom lies in the pπ orbital perpendicular to the σ bonding plane. The π orbital creates a weak π bond with π orbital in adjacent atoms. In sp^1 configuration two of the four electrons enters to form σ bonding while the other two enters pπ orbitals (Robertson 2002).

Variety of bonding configurations gives carbon allotropes different structures and properties unique from each other. Figure 2.2 shows different allotropes of carbon. Extreme physical properties of diamond are contributed to its highly directional σ bonds in sp^3 bonding configuration. Tetrahedral carbon bonds in diamond make carbon atoms form a unique face-centered-cubic (FCC) based structure. Some of the unique properties of diamond include extremely high hardness, high chemical inertness, low electrical conductivity, high transparency and high atomic density. Graphite on the other hand has properties widely different from diamond by virtue of its sp^2 bonded structure. Graphite has layered structure in which carbon atoms are covalently bonded together to form hexagonal units. The layers are connected by weak Van der Waals forces. Graphite is soft, highly conductive, black in color, and less chemical inert than

diamond. However both diamond and graphite has high industrial significance for different purposes.

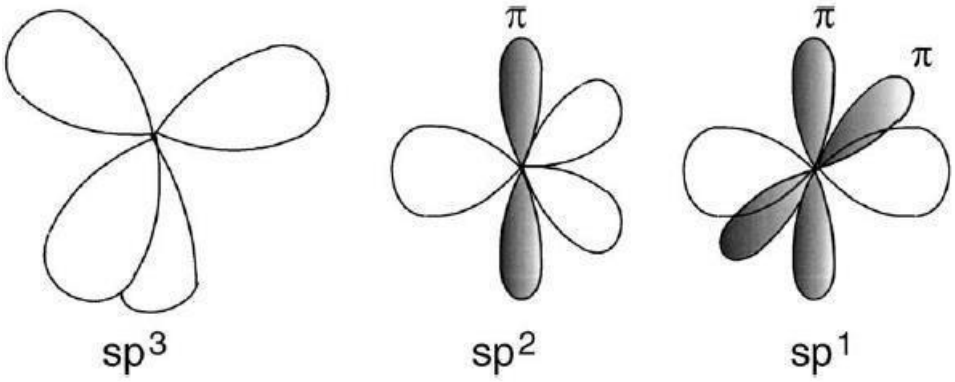

Figure 2.1 Different bonding configurations of carbon (Robertson 2002)

Carbon can also exist in the form of various nanostructures such as carbon nanotubes, buckminsterfullerene (C60), graphene, and nanofoams or as amorphous carbon (a-C). C60 has a structure similar to a soccer ball with sixty carbon atoms covalently bonded in hexagonal and pentagonal rings. It mostly finds application in photovoltaics. Carbon nanotubes have a cylindrical nanostructure with a single rolled layer or multi-rolled layers of one atom thick graphite sheet. Nanotubes are of sp^2 hybridized structure and characterized by extremely high strength and thermal conductivity. a-C contains random network of carbon atoms with different bonding configurations: combination of both sp^3 and sp^2. Amorphous carbon can have a wide range of properties depending on the bonding configurations and can be either diamond-like or graphite-like. a-C with relatively high amount of sp^3 bonding imparts diamond-like property while high fraction of sp^2 gives graphite like properties (Casiraghi et al. 2005).

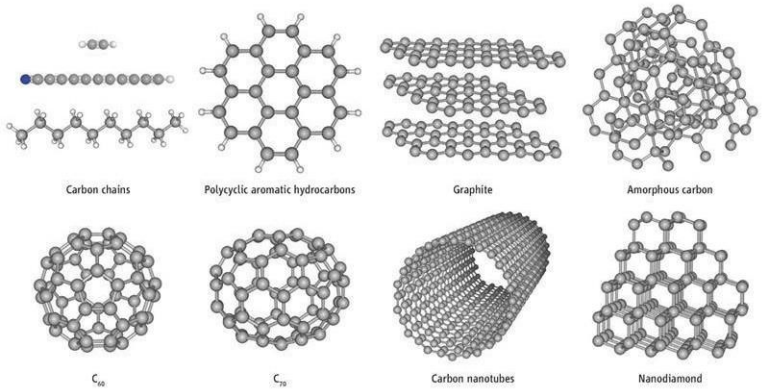

Figure 2.2 Different allotropes of carbon

2.2 Diamond- like Carbon Thin Films

2.2.1 Structure and Characteristics

Diamond-like carbon (DLC) refers to metastable amorphous carbon with relatively high percentage of sp^3 bonding in its structure (Grill, 1993). DLC can be broadly classified into two major categories: hydrogenated DLC and hydrogen free DLC. For hydrogenated DLC or hydrogenated amorphous carbon (a:C-H) the hydrogen percentage can vary between 10% to 60%. In general they have moderate amount of sp^3 bonding with high percentage of hydrogen terminated sp^3 bonds (C-H bonds). Hydrogenated tetrahedral amorphous carbon (ta:C-H) has relatively low (C-H bonds) and high amount of (C-C bonds) with sp^3 bonding as high as 70%. Hydrogen free amorphous carbon (a-C) has higher proportion of sp^2 bonding compared to a:C:H. Hydrogen free tetrahedral amorphous carbon has the highest percentage of C-C sp^3 bonds and can havehardness close to diamond (Casiraghi et al. 2005). Ternary phase diagram of DLC films has been illustrated in Figure 2.3. From the diagram we can predict the structure of DLC based on two major factors: sp^2/sp^3 bond ratio and hydrogen content.

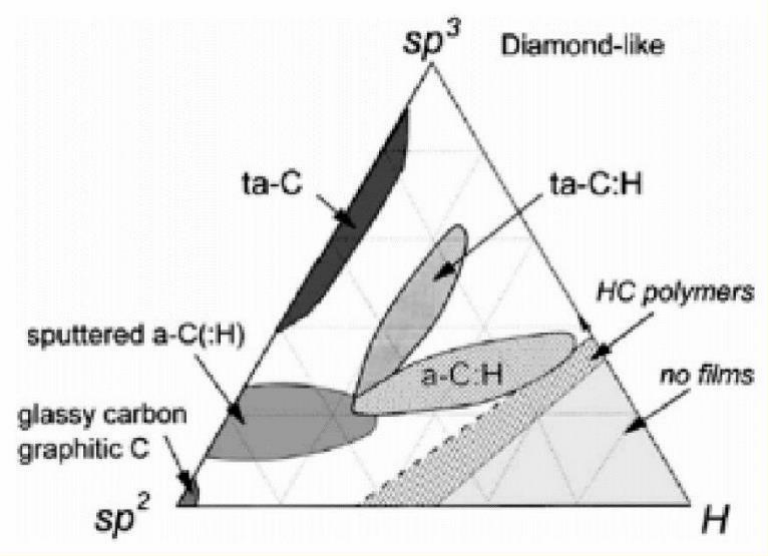

Figure 2.3 Ternary phase diagram of different DLC films (Box & Scala, 1995)

A relatively simple π-cluster model has been proposed to explain the electronic and mechanical properties of DLC (Fasel et al. 1997). According to this model, DLC comprises of a mixture of sp^3 and sp^2 bonds. The sp^3 sites form σ bonds while the sp^2 sites have π bonds. An isolated sp^2 site with its isolated π bond is highly unstable and thus enters to form a six-fold rings which consequently form aromatic cluster to stabilize. This planar sp^2 areas are non-homogenously distributed and connected by a network of σ bonds. The π bonds control the electronic properties while the σ bonds determine the mechanical property and hardness. However the cluster model is inappropriate for explaining the structure of amorphous carbon (a-C) containing very high amount of sp^2 sites because high amount of sp^2 prevents the clusters from being independent. The sp^2 sites are highly convoluted and the hardness can arise from interlayered bonding as sp^3 fraction is too low (Box & Scala, 1995). Figure 2.4 shows the theoretically suggested cluster model where the sp^2 clustered rings are interconnected by chains of sp^3 bonded atoms.

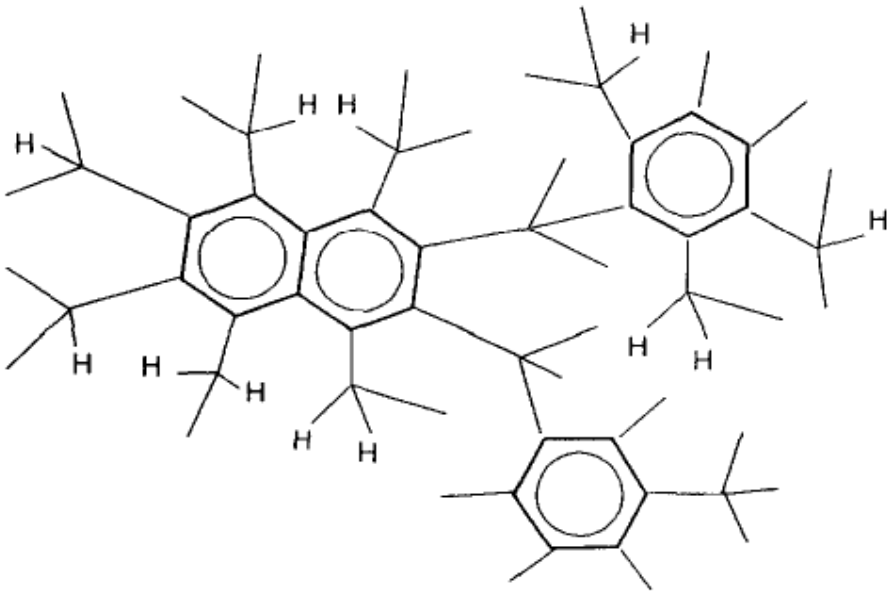

Figure 2.4 Cluster model in a:C-H film (Graner & Glazier, 1992)

Detailed analysis of the microscopic structure of DLC by tight-binding molecular dynamics (TBMD) simulation shows tetrahedral bonding sites are dominant component of the network (Graner & Glazier, 1992). Figure 2.5 shows schematic structure of a-C films generated from molecular dynamics simulation where the red spots represent the sp^3 sites and blue ones sp^2 sites. According to this model, DLC synthesized from graphite source in mass-selected-ion-beam (MSIB) are found to be dominated by tetrahedral sp^3 bonded atom. Most of the four fold atoms are surrounded by other fourfold atoms and some of them are surrounded by nearby three fold defects.

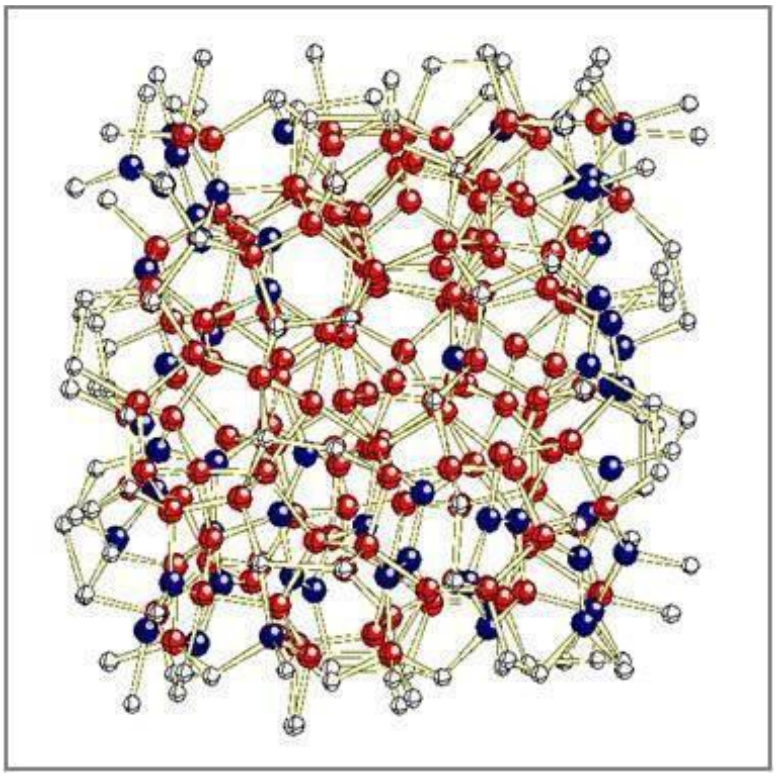

Figure 2.5 Microscopic structure of TBMD generated a-C network (Graner & Glazier, 1992)

The above models are just theoretical attempt to explain the structure-property correlation. Comprehensive structure of DLC at atomistic level has not yet been concluded. However previous studies show that the structure, chemical composition and properties of DLC can vary widely depending upon deposition methods, processing parameters and precursors used. For example, hydrogenated DLC synthesized from hydrocarbon source such as methane, ethane or benzene generally has high content of hydrogen whereas DLC produced from pure carbon sources has negligible hydrogen concentration (< 5%). It is hard to synthesize hydrogen free DLC and even the non-hydrogenated DLC coatings have some amount of hydrogen in it (Berkeley, 2001).

2.2.2 DLC Deposition Techniques

Synthesis of DLC dates back to 1971 by two researchers Aisenberg and Chabot using a relatively simple configured ion beam deposition system. The mean ion energy used in their experiments

was 40 eV(Aisenberg & Chabot, 1971).This work provided an impetus for further development of DLC/amorphous carbon coatings. Through the years a variety of chemical vapor deposition (CVD) and physical vapor deposition (PVD) approaches have been developed to meet the demand of various applications. These approaches include sputtering, ion beam assisted deposition, mass selected ion beam (MSIB), ion assisted evaporation, pulsed laser deposition, arc discharge and plasma enhanced chemical vapor deposition (PECVD) (Erdemir and Donnet 2006; Robertson 2002). Thus DLC has evolved as a new type of coating with excellent properties and could be synthesized much easily compared to diamond coatings. Figure 2.6 schematically illustrates some of the deposition methods. A particular synthesis process is chosen depending on the coating application. Each method has its own advantages and disadvantages in terms of the coating quality, deposition rate and uniformity. The deposited DLC thin films can have a wide spectrum of structure and properties depending on the specific deposition conditions.

Sputtering deposition is one of the most widely used industrial techniques for deposition of DLC (Robertson 2002). This technique finds widespread applications due to the variety of materials that can be easily sputtered. The major advantage of this technique is that deposition condition can be easily controlled by plasma power and gas pressure. Besides, they are reasonably independent of substrate geometry. In this momentum transfer process the energetic ions are used to sputter carbon species from pure carbon target. The generated carbon plume has a wide spectrum of energy depending on the mass and energy of the bombarding species (Robertson 2002). Direct current (DC) and radio frequency (RF) sputtering are most commonly used but other variants are also used include magnetron sputtering, ion beam sputtering and reactive sputtering. In magnetron sputtering the magnets are placed behind the targets increasing the rate of ionization and hence the deposition rate. In ion beam sputtering, the argon ions are generally used to bombard a graphite target to create carbon flux for deposition. Reactive sputtering is mainly used to synthesize hydrogenated DLC (a:C-H) using a mixture of plasma argon and hydrogen or methane. Disadvantage of the sputtering process involves its low ratio of energetic ions to the neutral species. DLC synthesized by this technique has low hardness which is unsuitable for some purposes.

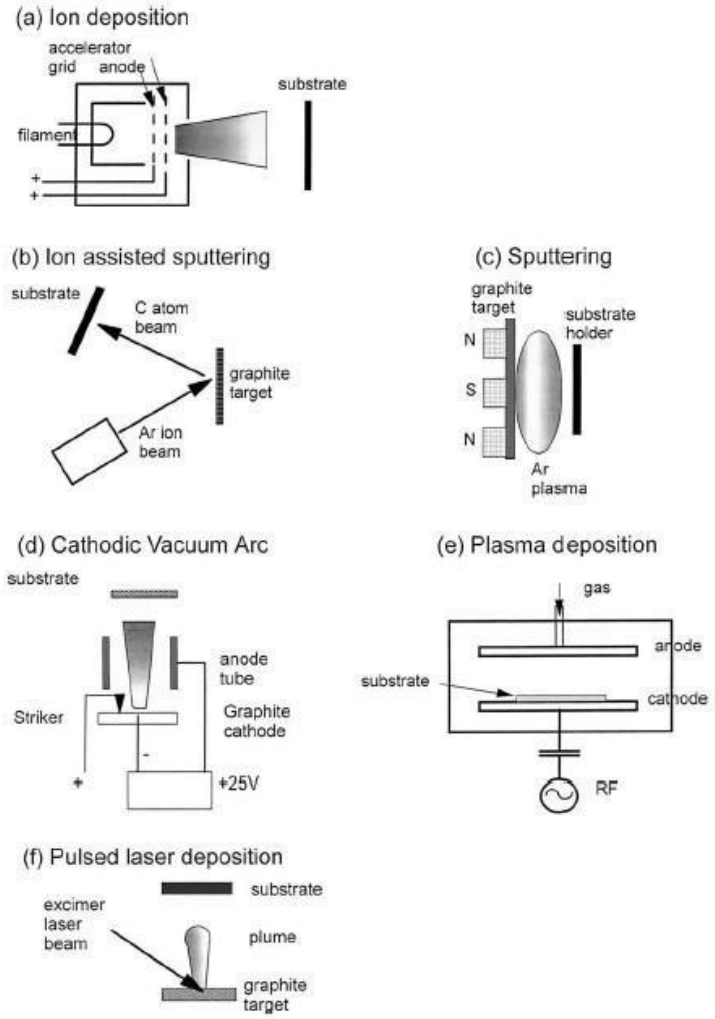

Figure 2.6 Schematic of different DLC deposition systems (Robertson 2002)

Arc discharge technique is used to produce DLC with high purity. The method utilizes electric discharge between anode and carbon cathode operated in a pulsed or DC mode. Laser arc method uses additional laser to ignite the spark between electrodes. High density carbon plasma with average energy of 30 eV can be generated. Doping elements into DLC is also feasible by this technique by either gas introduction or adding dopant to the cathode.

Mass selected ion beam (MSIB) is a special type of ion beam deposition which can precisely control deposition from single ion species within a well-defined ion energy. Carbon ions are produced from graphite target with minimal spread of the ion energy. The greatest advantage of this deposition method lies in its ability to deposit desired species while filtering out non energetic

species. MSIB however is not a commercially successful deposition method because of its extremely low deposition rate and high cost (Robertson 2002).

Pulsed laser deposition is a very effective PVD technique. In this method generally pulsed ArF laser is employed to strike a small area of the target material. The high intense laser pulses causes the material to be vaporized as an intense plasma. The mean ion energy of the plasma is directly proportional to the laser fluence focused at the target spot. This method is considered one of the most versatile method producing high quality DLC. This laboratory scale technique is used to deposit coatings for applications from high temperature semi-conductors to hard coatings(Robertson 2002).

In PECVD method a glow discharge is used to activate gas molecules required for synthesis. Different hydrocarbon gases like methane, acetylene, benzene, propane and ethane have been employed to synthesize DLC using this technique.

In a typical ion beam deposition, carbon ions are produced by plasma sputtering of the graphite target or a hydrocarbon gas such as methane, which can be ionized by mostly Kaufman Ion Source. The carbon ions are then accelerated to form the ion beam in high vacuum deposition chamber. However the ion beam in this case contains a large amount of high unionized gases reducing the flux ratio of ions to the neutral species. The amount of sp^3 fraction obtained by this technique is limited (Robertson 2002).

2.2.3 Deposition Mechanism

The unique properties of DLC are attributed to its sp^3 C-C bonding network. It is formed by the bombardment of the energetic ions where the energetic ions are implanted in the sub-surface (below the top surface) in a densified layer, in which, the energetic ions enter into metastable sp^3 configuration rather than more stable sp^2 configuration (Robertson 2008). Energy of the carbon ions for amorphous carbon coating generally lies in the range of 10eV – 1000eV (Lifshitz, 1999). Thus the growth of the amorphous carbon coating follows shallow implantation (“sub-plantation”) process rather than surface condensation process. Since the deposition process largely depends on

the incoming energetic ions so it is not thermally activated. This gives DLC a high practical advantage over other coatings like diamond as they can be deposited at room temperature (Robertson 2008). The popular sub-plantation growth mechanism proceeds through four stages (Lifshitz, 1999).

- Implantation of the carbon atoms in the sub-surface layers
- High density of carbon atoms in the sub-surface inducing local stresses
- Dilution of the target atoms until a pure carbon layer evolves
- Gradual growth of the carbon layer upon successive bombardment

For the sub-plantation growth carbon ions must pass through the interstices and penetrate the surface. The ion energy required for this activity is called penetration threshold E_p. However, the surface atoms are tightly bonded to each other and thus the incoming ions need minimum amount of energy to displace an atom from its site and create a permanent vacancy-interstitial pair. The minimum energy required by an ion to do this is called displacement threshold E_d. The binding energy which hold the surface ions are denoted as E_b. Thus for a group of carbon ions with certain critical energy, the net penetration threshold is defined by

$$E_p \sim E_d - E_b \tag{2.1}$$

The ions having energy lower than the penetration threshold will not be able to penetrate and stick to the surface to form sp^2 bonds. When the ion energy is greater than the E_p it can penetrate into the subsurface. At the subsurface they increase the local density. High amount of energetic ion bombardment increases the local density giving rise to high amount of sp^3 bonding. With the increase in the ion energies most of the ions penetrate deeper into the subsurface while some ions get involved in displacement of the surface ions. The entire process of sub-surface implantation consists of collision, thermalization and relaxation (Robertson 2002). However, when the ion energy is over a certain value, the excess energy of the ions are lost as heat, causing local relaxation, subsequently decreasing the sp^3 bonding.

Figure 2.7 schematically explains the sub-plantation growth mechanism. The incident beam shown has certain fraction ϕ with energetic ions. Fraction of the energetic ions ϕf has energy greater than

the penetration threshold (E_p) and penetrates the surface occupying the *n* fraction of interstitials. The fraction (*1- ϕf*) has ions with energy less than the penetration threshold and mostly resides on the surface. Some of the penetrating ions will relax back to the surface as shown by the relaxing fraction nβ. In a steady state condition number of ions remaining for densification is given by the equation,

(2.2)

$n = \emptyset f - n$

where β is a constant.

$$n = (\emptyset f)/(1 + \beta) \quad (2.3)$$

where *n* represents the fraction of the beam that gets sub-planted whereas the other fraction of the beam *(1-n)* is left on the surface as growing sp^2 layer. The sub-plantation density increase is given by

$$\Delta\rho/\rho = n/(1 - n) \quad (2.4)$$

Substituting the value of *n* in the above equation,

$$\Delta\rho/\rho = (\emptyset f)/(1 - \emptyset f + \beta) \quad (2.5)$$

where $\Delta\rho$ is considered as the density increase and ρ is defined as the density of sp^2 carbon. The outward growing layer is the sp^2 layer while the subsurface layer mostly is sp^3 hybridized carbon.

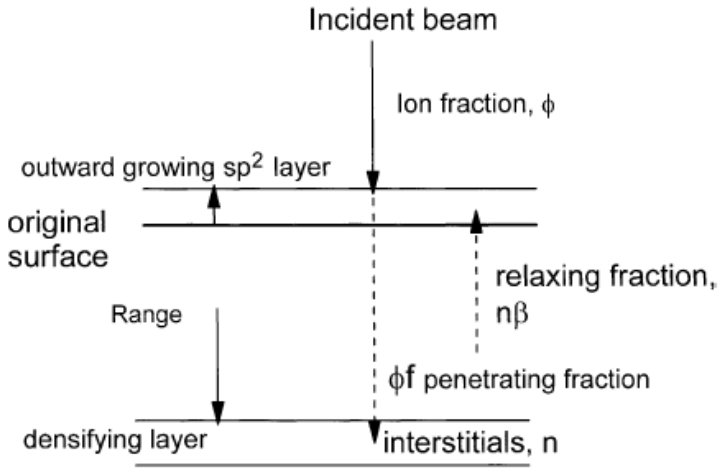

Figure 2.7 Schematic Diagram of the sub-plantation growth (Robertson 2005)

Growth of a-C:H Films: The growth of hydrogenated carbon films also follows the basic sub-plantation growth model, however the mechanism in this case is slightly more complex than a-C films. Hydrogenated carbon films can be synthesized from different hydrocarbon precursors like benzene, methane, ethane, propane and acetylene. The entire growth process of hydrogenated carbon films can be divided into three basic steps:- (a) reactions in the plasma such as dissociation or ionization; (b) plasma reacting with the surface of the growing film and (c) sub-surface reactions in the film. The reactions in the plasma generate ions and also neutral species. The neutral species can be un-dissociated precursor gas, mono-radicals (CH_3), di-radicals (C_2H_4), unsaturated species and also atomic hydrogen. Both neutral species and ions contribute towards the film growth. Di-radicals along with other unsaturated species in the plasma enters mostly the C-H bond and C-C bonds on the surface. The mono-radical contribution to the growth rate is comparatively less as they cannot directly form a bond. Mono-radicals can only react on the film surface in the presence of an existing dangling bond. Hydrogen has a very significant role in the chemistry and growth of hydrogenated amorphous carbon. Hydrogen atoms being smaller than the radicals, weakly interact with the carbon atoms and penetrate deeper in the film. Hydrogen atoms can then abstract other hydrogen from the C-H bonds to form hydrogen molecule and subsurface unsaturated dangling bonds. Thus the entire process of growth of hydrogenated amorphous carbon consists ofchemical procedures of the various species in the plasma, dehydrogenation-recombination and sub-

plantation of the energetic ions. Figure 2.8 shows the growth model of hydrogenated amorphous carbon as suggested by Robertson.

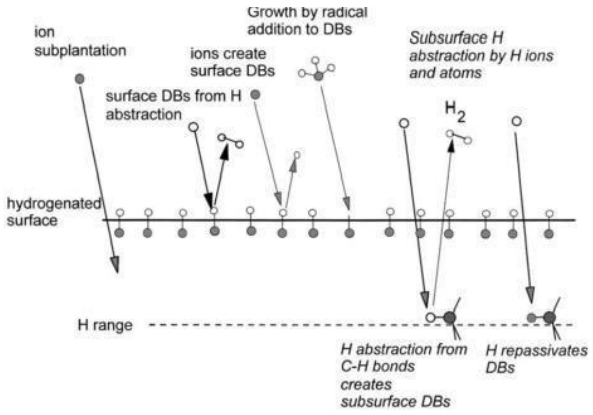

Figure 2.7 Model of growth process in a:C-H (Robertson 2002)

2.2.4 Stresses in DLC

Because of the bombardment of energetic species, high amount of residual stresses(compressive) exists in the coating and increases with the increasing of film thickness (Peng & Clyne, 1998). Stresses developed in DLC during its synthesis is highly undesirable for industrial application as it leads to poor adhesion and premature delamination of the coating, especially on metallic substrates. The residual stresses in DLC can be broadly classified into three different categories depending on the originating sources (Fontaine et al. 2008):

(a)) thermal stresses,

(b) intrinsic stresses and

(c) extrinsic stresses.

2.2.4.1 Thermal Stresses

Elevated deposition temperature and thermal coefficients mismatch between the coating and the substrate are predominant factors generating thermal stresses in the coating. Deposition carried out

at elevated temperatures can cause uneven thermal expansion of the coating and its substrate inducing high amount of stress eventually leading to failure of the coating. Thus for DLC deposition it is highly desirable to carry out the deposition at room temperature to eliminate any thermal stresses. Pre-deposition of interlayer is one of the widely used method to minimize such kinds of stresses in the coating (Wei et al. 2009).

2.2.4.2 Intrinsic Stresses

Intrinsic stresses are related to the morphology and microstructure of the coating. Thus intrinsic stresses vary largely depending on the deposition parameters and processes. Intrinsic stresses in a coating can be broadly classified into two types: tensile intrinsic stresses and compressive intrinsic stresses. Tensile intrinsic stresses are usually caused by defects such as vacancies, voids, in the coatings.

Compressive intrinsic stresses are dominant in the coatings deposited with the bombardment of energetic particles (Fontaine et al. 2008). The energetic particle bombardment modifies the structure of the coatings eliminating the sources which gives rise to intrinsic tensile stresses. Compressive stresses progressively increases to a certain maximum value with increasing impact energy per atom. According to a model proposed by Davis, implanted atoms at the subsurface through knock- on processes gives rise to compressive intrinsic stresses. Figure 2.9 shows the difference between energetic ion implantation by direct entry and knock on processes. The energetic ions implanted into the subsurface moves into a metastable position. However bombardment from other energetic species causes intense local heating in certain areas due to energy transfer among the atoms. Local heating provides energy to the atoms to form a stable structure, causing relaxation when cooling down. This energy provided from heating is called 'thermal spike'. Compressive stress thus greatly depends on the balance between implantation and relaxation and is proportional to the ratio of ion flux (ϕ_i) to deposition rate (ϕ_d) (Fontaine et al., 2008; Pauleau, 2001). Films produced by low normalized fluxes (ϕ_i/ϕ_d) with low kinetic energy and high deposition rate lowers compressive stress. However coatings manufactured by this

process usually have lower hardness. Similarly films synthesized with high normalized fluxes (ϕ_i / ϕ_d), high deposition energy and low deposition rate show high compressive stresses (Fontaine et al. 2008). Alternatively incorporation of elements into films (doping) with flexible bonding states showed significant improvement in the coating quality with reduced compressive stresses (Bilek & McKenzie, 2006). For example past studies showed that doping amorphous carbon/DLC with various elements significantly reduced compressive stress without compromising its attractive properties (Erdemir & Donnet, 2006).

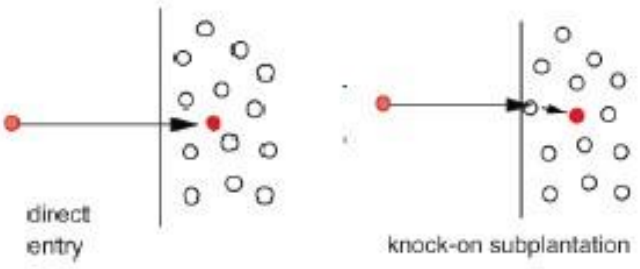

Figure 2.8 Implantation of energetic ions in growing films (Fontaine et al. 2008)

2.2.4.3 Extrinsic Stresses

Extrinsic stresses are generated by interaction of the external factors with the deposited film. This can be caused by unwanted incorporation of oxygen or hydrogen from the environment which reacts with the coating material to produce phases with different volume. Phase transformations can also lead to volume changes and thus generating stress in its vicinity.

2.3 Applications of DLC

DLC is one of the widely used coatings for indutrial applications due to its unique set of properties such as high hardness, high chemical inertness, excellent bio-compatibility, low friction

coefficient, low wear rates, transparency in infrared and visible light, extremely smooth surface and its ability to be deposited at room temperature (Lifshitz, 1999). DLC coated on magnetic hard disks eliminates high wear of the disk while sliding against the head giving a prolonged life before failure. DLC coated razor blades had shown superior performance than conventional blades. DLC showed promising characteristics in optics industry and is widely used as protective coatings on germanium and zinc sulphide windows. DLC has also found extensive use in the solar energy sector (Lettington, 1998).

Aerospace systems often face challenges such as high friction and wear of the moving components such as reaction wheels, antenna drives, gears pumps, actuators and latches. DLC is a relatively new coating material in aerospace industry which significantly improved the lifetime of the aerospace parts. Further investigations into synthesis of composite DLC coatings have been carried out to obtain a desirable combination of hardness, toughness and friction and wear properties (Voevodin et al. 1999) for a wider applications. For example, DLC has been extensively used to coat engine parts in automobile industry, primarily due to its high high wear resistance and low friction coefficient, thusmuch less consumption of energy; DLC films are also employed in the manufacturing and chemical industries due to its high chemical inertness and excellent tribological property (Lifshitz, 1999).

DLC emerges as one of the most favourable coatings in bio-medical industry. Due to increasing medical demands, a variety of medical implants such as knee and hip joints, heart valves, coronary stents are used in the human body. Biomaterials are generally made up of polymers, metallic alloys (cobalt-chromium alloys, stainless steel, titanium alloys) or ceramics (zirconia and alumina). In its entire lifetime biomaterials are subjected to various mechanical loading and exposed to harsh chemical environment when interacting with the body fluids. Metallic implants such as titanium and chromium tend to release metal ions and wear debris in such harsh conditions. This may lead to tissue inflammation and osteolysis gradually causing loosening of the implant and its failure (Grill, 2003). DLC based coatings by virtue of its high hardness, high chemical inertness, high wear resistance and excellent biocompatibility have potentials to be used as coating material in bio-medical industry. Enhanced service performances of various DLC coated bio-materials has already been reported (Lettington, 1998; R. K. Roy & Lee, 2007; Srinivasan et al. 2012).

2.4 Adhesion of Coatings

Adhesion to the substrate determines the protective efficiency of a coating. Elastic energy per unit volume of the coating, intrinsic stress in the coating, and interfacial energy between the coating and substrate are important factors which control the adhesion of the coating to the substrate. The instability between the coating-substrate system occurs when the stored elastic energy exceeds a certain critical value.

Schematic diagram in Figure 2.10 shows surface free energy change when coating delaminates from the surface. For a perfectly adhered coating-substrate system the work done by adhesion is given by γ_a. Complete delamination of the coating from the substrate produces two new surfaces, one for the coating with surface energy γ_c while the other for the substrate with surface energy γ_s. Thus in ideal situation the work done by adhesion is given by,

$$\gamma_a = \gamma + \gamma_s \tag{2.6}$$

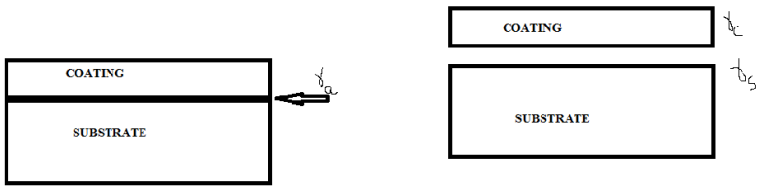

Figure 2.9 Surface free energy change when coating delaminates from substrate

Films produced by energetic techniques exhibits high amount of intrinsic compressive stresses. After a certain maximum stress level, buckling phenomenon initiates at a site of defect. Buckling releases the excessive compressive stress in the deposited film. The elastic strain energy released due to buckling provides a driving force for delamination. The elastic energy (U) is related to the compressive stress by the equation 2.7,

$$U = \frac{(1-\nu)h_c\,\sigma^2}{E_c} \tag{2.7}$$

v_c= poisson ratio of the coating

h_c= thickness of the coating

E_c= elastic modulus of the coating

σ = residual stresses in the coating

When the stored elastic energy in the film exceeds the critical value (U_c) and becomes equal to the work done by adhesion, the coating- substrate system destabilizes and the coating delaminates. Combining equations 2.6 and 2.7 gives the correlation between the critical stress and the thickness of the coating.

$$\frac{(1-\nu_c)h_c\sigma^2}{E_c} = \gamma_a \quad (2.8)$$

Assuming that the surface energies of the coating and the substrate are identical, equation 2.6 becomes,

$$\gamma = 2\gamma_a \quad (2.9)$$

Thus substituting the values in equation 2.8 into equation 2.9 gives,

$$\frac{(1-\nu_c)h_c\sigma^2}{E_c} = 2\gamma \quad (2.10)$$

The critical thickness for the coating at a particular residual stress is given by (Fontaine et al., 2008),

$$h_c = \frac{2\gamma E_c}{(1-\nu)^2\sigma^2} \quad (2.11)$$

According to the above equation coating will have excellent adhesion if the surface energy of the coating –substrate system is high or the residual stress is highly reduced. DLC with its high internal

compressive stress normally adheres poorly on bare substrates. Past investigations of DLC deposition on bare stainless steel substrates showed poor adhesion due to the high residual stress

and mismatch of the interface (Chang & Wang, 2001). The adhesion significantly improved with a single interlayer and a functionally graded interlayer which is mainly due to close resemblance of the properties of DLC with interlayers. DLC deposited on a bare titanium alloy (Ti-6Al-4V)

showed similar poor adhesion and a silicon interlayer was used to enhance the adhesion of DLC on the substrate (Kim et al., 2005). Various other approaches such as plasma treatment of the substrate surface, incorporation of the metallic (Ti, Cr, W) and non-metallic (N, F, S) elements were made in an attempt to reduce the internal compressive stress of DLC (Donnet, 1998). Recent investigation of nano-diamonds incorporated DLC on a titanium alloy showed enhanced adhesion (C. Z. Zhang et al. 2013). It has been found that the pre-deposited nano-diamond particles greatly increase the interfacial bonding on Ti substrate by forming titanium carbide, which reduces property mismatch between the substrate and the coating mismatch. Thus modified DLC by element doping along with pre-deposited nanodiamond particles could serve as a potential method for producing good quality protective coatings on metallic substrates specially titanium alloys.

2.5 Alloyed DLC

Doped DLC thin films forms a special class of amorphous carbon coating with enhanced properties. The amorphous nature of DLC makes it easier to be doped with various metallic and non-metallic elements thus enhancing properties such as thermal stability, hardness, internal stress, tribological property, surface energy and bio-compatibility. Doping of various elements into DLC and its influence on different properties are schematically shown in Figure 2.11. The modified DLC coatings are synthesized in a similar way as pure DLC by addition of the doping species in the deposition environment. The composition of the doped element and properties of the modified DLC varies depending on the parameters and deposition technique used.

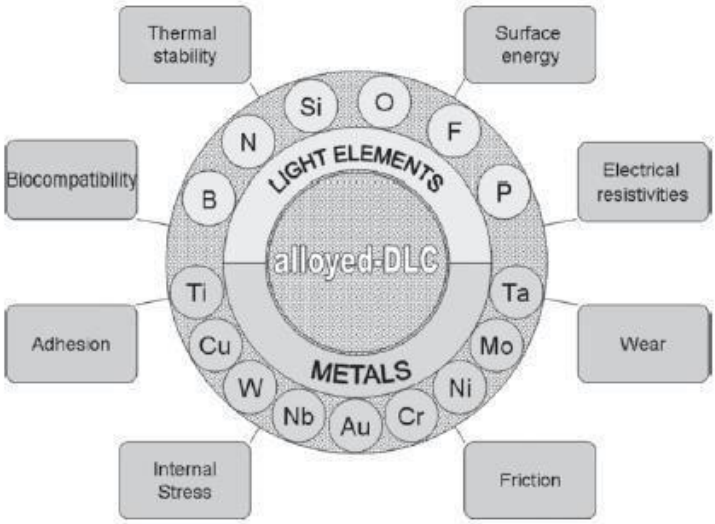

Figure 2.10 Doping of various elements in DLC (Erdemir & Donnet, 2006)

2.5.1 Metal doped DLC

Researches on doped DLC with various metals have been carried out in past decades. The choice of a particular metal to be doped depends on the application. Singh et al. reported increased micro-hardness in chromium doped DLC. Atomic clusters of chromium carbide dispersed in DLC matrix significantly enhanced the wear resistance of DLC coating (Singh et al., 2006). Titanium is another metallic element of high interest and like chromium is a strong carbide forming element. A large number of past works on Titanium doped DLC showed enhanced adhesion, thermal stability and mechanical properties due to dispersed TiC in DLC matrix (Ma et al. 2012). Nickel doping increases both electrical conductivity and adhesion, reduces wear, and stabilize coefficient of friction (Ma et al. 2010). DLC doped with metals in general are characterized with lowerinternal stress, higher elastic modulus, higher hardness, higher wear resistance and lower steady friction coefficient compared to pure DLC, which can be attributed to the dispersed carbide phases in DLC matrix.

2.5.2 Non-metal doped DLC

DLC has also been doped with various non-metallic elements such as silicon, boron, fluorine and nitrogen by various PVD and CVD techniques. Silicon doped DLC has extremely low friction coefficient and wear rates in ambient air and dry nitrogen serving as a great candidate for tribological applications (Donnet, 1998). The lower coefficient of friction of silicon doped DLC is mainly due to the formation of SiO_2 phase at the surface. But too high concentration of Si in DLC can lead to high internal stress and cracking (Wu et al. 1998). Fluorine doped DLC has also been studied by many researchers. However fluorinated DLC (F-DLC) failed to improve the good properties of DLC. Fluorinated DLC is reported to have lower hardness than conventional DLC due to formation of the $–CF_2$ and $–CF_3$ bonds which reduces the density of the coating. High fluorine content in DLC renders it soft and subsequently reduces its wear resistance, thoughsome reports F-DLC deposited on magnetic recording media showed improved micro-wear and reduced friction coefficient within short time (Donnet, 1998). Doping of boron into DLC increases its electrical conductivity and hardness by promoting C-C sp^3 bonding (Zhang 2012).

2.5.3 Nitrogen Doped DLC

Nitrogenated DLC (N-DLC) forms an interesting class of DLC and has various applications**.** Nitrogen doping in amorphous carbon gained significant interest in the past decades due to its versatile properties. Nitrogen doping into DLC was initially inspired by the idea of synthesizing theoretically predicted β-C_3N_4 structure (Hu et al. 1998). In their work, it was proposed that β-C_3N_4 could have hardness and bulk modulus similar to diamond. For a stable β-C_3N_4 phase the carbon atoms should have sp^3 atomic configuration while nitrogen should be sp^2 bonded. Also nitrogen content should be high enough to maintain the 4/3 stoichiometry in the carbo –nitride compound. However achieving such phase is practically difficult due to the high stability of nitrogen to nitrogen triple bond which makes nitrogen more susceptible to form N_2 even within a solid. Till date practical evidence of such a phase has not been reported (Dwivedi et al. 2011).

However investigations on nitrogen doped DLC showed huge potential for industrial applications as it has reduced stress, high hardness and excellent tribological properties (Grill, 1997). Nitrogen

incorporation into DLC matrix promotes N-H and C-N bonding at the expense of C-C debonding (Dwivedi et al., 2011). Depending on the deposition parameters and concentration of nitrogen other types of C=C and C=N can also be present in a nitrogenated DLC (Sánchez-López & Fernández, 2008). At lower nitrogen content nitrogen tends to enter N-sp^2 C bonding however when doping percentage increases it tends to form more N-sp^3 C (Zou et al., 2005). Decrease of sp^3 C-C bonding decreases the average coordination number of carbon in nitrogen doped DLC and thus reduces the internal stress (Kumar, Dixit, Sarangi, & Bhattacharyya, 1999). Investigations by Cheah et al. on nitrogen doped DLC showed similar reduction of internal stress and lowered hardness with increasing nitrogen content (Cheah et al., 1998). In another study of nitrogenated DLC deposited using ion beam deposition by Sethuraman et al showed increased hardness compared to conventional DLC (Srinivasan et al., 2012). Owing to the excellent properties of nitrogenated DLC considerable investigations have been carried out by researchers but systematic study is still required to fully understand the structure –property correlation for extensive industrial applications. Especially, very limited studies are performed on nitrogenated DLC deposited using low energy E-H (End Hall) ion beam source. Thus it would be interesting to study the properties of nitrogenated DLC synthesized by EH ion source.

2.6 Chemical and Structural characterization of DLC coatings

2.6.1 Raman Spectroscopy:

Visible raman spectroscopy is one of the most important non-destructive characterization techniques for carbon coatings. Raman spectra is widely being used for analyzing the bonding structure of DLC. The technique works on the principle of Raman Effect which is inelastic scattering of indicident monchromatic light when it interacts with the molecules, atoms or crystal lattices. Raman shift is caused due to the energy difference between the incident photon and scattered photon and can be used to identify a particular substance or a bond because different molecules have different vibrational modes. Figure 2.12 shows schematic of Raman scattering from a molecule. The plot of intensity of the scattered light versus the Raman shift (measured in cm^{-1}) is the Raman spectrum.

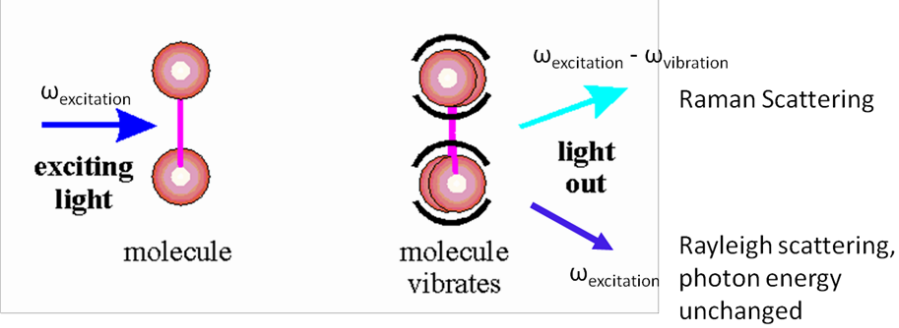

Figure 2.11 Raman Scattering from a molecule

Generally all carbon materials show characteristic Raman peaks in the region of 800-2000 cm^{-1}. Figure 2.12 represents typical Raman spectra of various carbon materials. Raman Spectroscopyis much more sensitive to sp^2 sites because of their higher cross sectional area. Diamond has a single Raman active mode at 1332 cm^{-1} and single crystal graphite has a Raman active mode at 1580 cm^{-1} and this peak is termed as "G" peak (Grill, 1997). Disordered graphite has a second Raman active mode at 1360 cm^{-1} labeled as "D". It is interesting to note that Raman spectra of almost all disordered carbon materials comprises of G and D modes of graphite even though the carbon atoms do not necessarily have the graphitic crystal structure. The G peak is contributed by the stretching of sp^2 bonded atoms in both rings and chains whereas breathing modes of sp^2 atoms in the rings contributes D band in the Raman spectra for amorphous carbon (Casiraghi et al. 2005). Intensity ratio of the D peak and G peaks in Raman spectra gives important bonding information about carbon coatings.

Being amorphous structures, DLC and N-DLC show very broad and overlapped D and G peaksin their Raman spectra (Srinivasan et al. 2012). Thus to obtain bonding information from Raman spectra of DLC fitting using Breit-Wigner-Fano (BWF)fitting method to fit the G peak and Lorentzian for D peak is required (Robertson 2002). As suggested three stage model of increasing disorder for Raman Spectra of various amorphous carbon. In stage one, it progressively changes from graphite to nano-crystalline graphite structures. This stage is marked by decrease in the grain size while maintaining the aromatic rings. In this stage the G band shows an upshift and generally goes up to 1600 cm^{-1}. The D band is insignificant in this stage as there is almost no disorder. Stage two is marked by change from nano-crystalline graphite structure to disordered sp^2 rich amorphous carbon network. This leads to the loss of aromatic bonding and shifting of the G-peak to a lower

wavenumber. Staged three is marked by change of sp^2 configuration from rings to short chainsand gradual increase of sp^3 content towards 100 %. In this stage intensity ratios I_D/I_G gradually approaches to zero with G peak position shifting down with the increase of sp^3 content. This gives us an estimation about sp^3 fraction in DLC (Fontaine et al., 2008). Raman Spectroscopic techniques can also be used to study the residual stresses in DLC. With compression the atomic vibrational frequency changes and this causes a shift in the position of the G peak. The residual stress is related to the G peak shift by the following relation (Fontaine et al. 2008).

$$\frac{(1+\nu_f)\Delta\omega}{f} \qquad (2.12)$$

$$\sigma = 2\omega_f{}_{(1-\nu}{}^{)\omega\omega}$$

In the above equation ω stands for shear modulus while v_f denotes Poisson's ratio of the film.

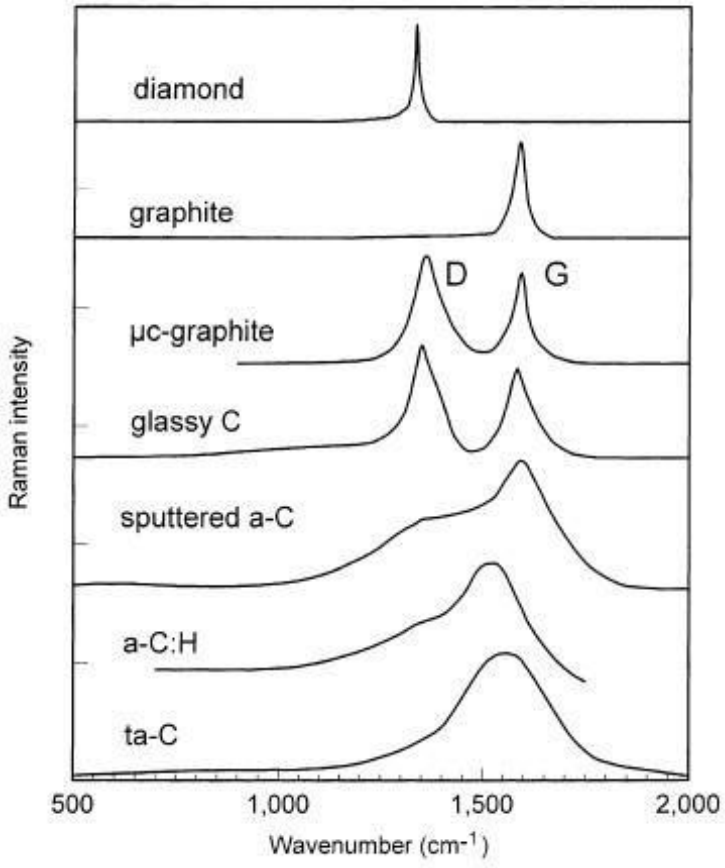

Figure 2.12 Raman Spectra of various carbon materials (Robertson 2002)

2.6.2 X-Ray Photoelectron Spectroscopy

As the name suggests, X-ray Photoelectron Spectroscopy (XPS) works on the principle of photoelectric effect. In this method electrons escaping out of the material surface after photon absorption is studied and corresponding binding energies are calculated. It is widely used to characterize elemental composition of a sample. The working mechanism of XPS instrument is schematically shown in Figure 2.13.

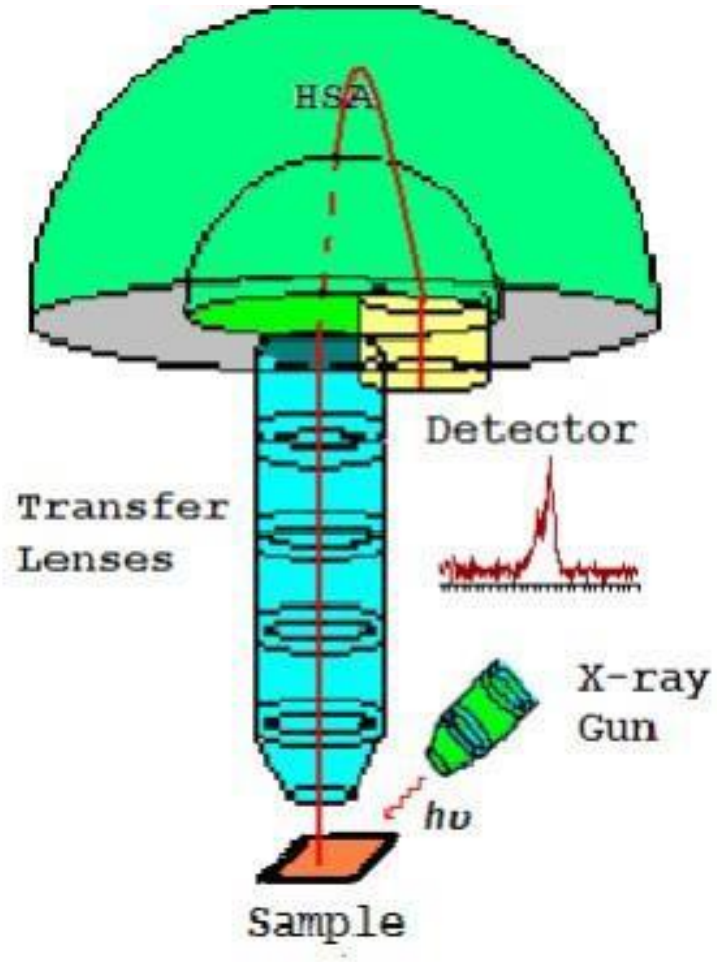

Figure 2.13 Schematic of XPS instrument (Xps, 2013)

In a conventional XPS system an X-Ray gun with photon energies between 1-2 keV is used to bombard the surface of the material. In the process the inner shell electrons of the target atoms get

excited and then emit photoelectrons. The photoelectrons emitted from the surface are then passed through the hemispherical analyzer (HSA) and then analyzed by the detector. According to Einstein's law, the energy of the absorbed photon is more than the kinetic energies of the emitted photoelectrons. This difference in energies is the binding energy of the electron which is characteristic for each element. Analysis of the measured kinetic energies of the photo electrons gives us the information about the elements present in the material. XPS analysis is highly surface specific and is not very useful to characterize elements present at bulk. This is because the bombarding X rays might have enough energy to penetrate deeper into the material but the escape depth of ejected electrons are limited. The ejected electron from deep into the surface experience energy loss and contribute to background signal rather than well-defined intensity peaks (Xps, 2013).

2.6.3 Near Edge X-Ray Absorption Fine Structure Spectroscopy (NEXAFS)

NEXAFS is widely used to study the local electronic structure of the material in solid, liquid or gas phases. NEXAFS is also called X-ray absorption near edge structure (XANES) but inmodern day NEXAFS refers to soft x-ray absorption spectra, that is, energy of the X-ray used for this study is lower than the one used for XANES. The term" absorption" in these measurements comes from the core shell from which the electron is excited such as K-edge, L-edge, M-edge respectively. In NEXAFS the X-ray with different energies is scanned and then the absorbed X-ray intensity from the samples is measured. NEXAFS spectra are often collected in two modes: fluorescence yield (FLY) and total electron yield (TEY) (Y. H. Tang et al. 2001). FLY mode is bulk sensitive and the probing depth could be up to tens of nanometers. In TEY mode the absorbed X-ray intensity is not measured directly but the photoelectrons and auger electrons that are created at the surface due to absorbed ray are counted. TEY is highly surface sensitive as the photoelectrons and auger electrons generated at a greater depth lose much energy due to cascade and do not contribute to the TEY spectra. NEXAFS is highly element specific as different element have different absorption spectra. NEXAFS also gives detailed information about local bonding and structure information.

2.7 Mechanical Characterization and Adhesion Testing

Mechanical properties of DLC plays a very an important role in engineering applications. Generally mechanical characterizations involve measurement of properties such as elastic modulus, hardness, and friction coefficient, and wear resistance. There are various techniques for measuring the mechanical properties of thin films. However nanoindentation is the most widely used one. In nano-indentation diamond tip is used for indentation with indentation loads varying from micro to milli Newtons depending upon experimental requirements. Nanoindenters are classified according to the their tip geometries such as Berkovich, Vickners and Knoop types and each of them has their own characteristics (Erdemir & Donnet, 2006) . The diamond tip is progressively forced in the film and the force displacement curve is measured. Loading and unloading curve of typical amorphous carbon film is represented in Figure 2.14. The values are obtained by drawing tangent to the unloading curve and then extrapolating it to zero. Hardness is given by $H = 0.0378\, L_{max} / h_p^2$

$$H = 0.0378 \frac{L_{max}}{h_p^2} \quad (2.16)$$

where the young modulus is proportional to the slope of the tangent and given by the equation

$$E = 0.179 \frac{(1-\nu^2)}{(h_{max} - h_f) h_p} \quad (2.17)$$

In the above equations L_{max} represents the maximum load, v the Poissons ratio, h_p represents plastic the deformation while the length of the intercept $h_{max} - h_p$ is the elastic deformation undergone by the film.

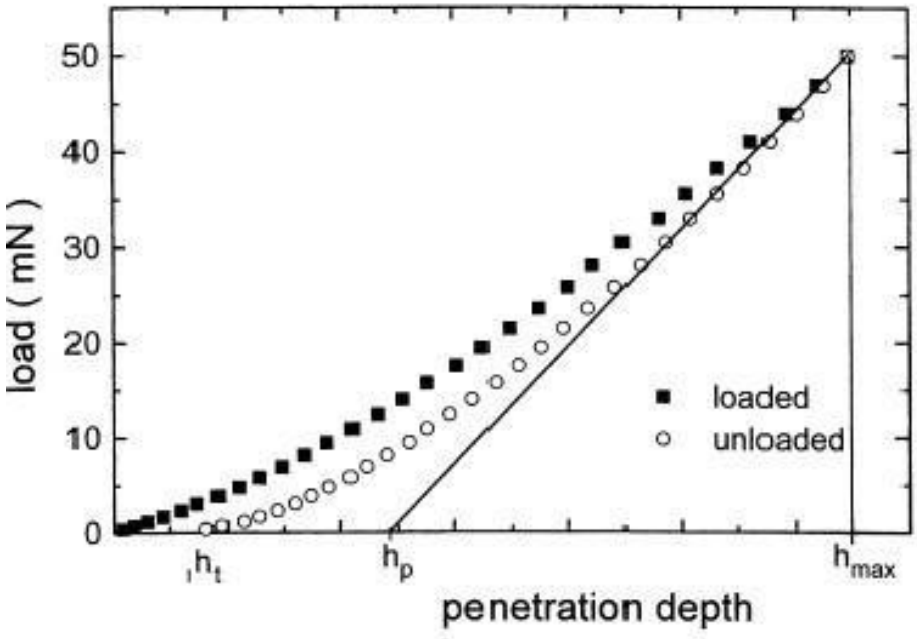

Figure 2.14 Loading –unloading curve for nano-indentation measurement (Robertson 2002)

Hardness is related to other mechanical properties such as yield stress (Y) and Young's modulus by the mathematical formula:

$$\frac{H}{Y} = 0.07 + 0.06\ln\left(\frac{E}{Y}\right) \quad (2.18)$$

For most of the ceramics and diamond the value of H/Y is close to 1.8. For coatings like DLC where yield occurs by bond cleavage and thus plasticity index (H/E) is used to determine the quality of the coating. Coatings with high values of H/E is considered to be high wear resistant such as DLC (Dwivedi et al. 2011).

Adhesion of the coatings to the substrate is one of the most important properties and numerous techniques such as tape test, pin pull test, and scratch test have been employed employed to test the adhesion of the coating to the substrate. Scratch and indentation testing are two most commonly

used methods for evaluating the adhesion of hard coatings to their substrates. In a scratch test a progressively increasing normal load is applied to the coating till it delaminates. Frictional forces and acoustic emission data are continuously monitored in scratch testing. The load at which the coating delaminates is shown by the acoustic signal and is known as critical load for delamination (Fontaine et al. 2008).

Rockwell C indentation tester is commonly used for adhesion measurement. A load of 1471 N is usually applied to the coating perpendicularly and after indentation the area around the indent is evaluated under microscope. The severity of damage adjacent to the boundary of indentation is compared with defined adhesion quality as standardized by VDI guidelines 3198,Germany (Heinke et al. 1995). Figure 2.15 shows the adhesion strength quality from HF1 to HF6. In Figure 2.15, HF1 to HF4 is considered sufficient adhesion according to the VDI guidelines whereas HF5 and HF6 represents insufficient adhesion of coating to substrate. In our present investigations, adhesion strength of our coatings are investigated by Rockwell C testing using a load of 1497N.

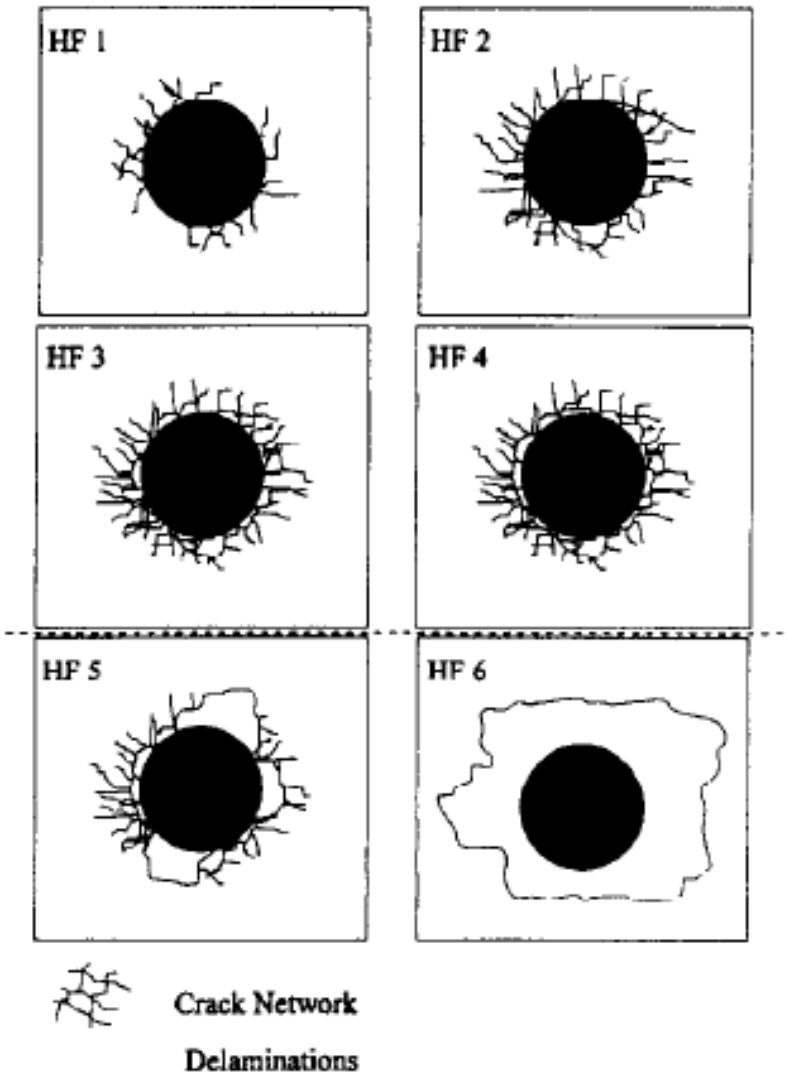

Figure 2.15 Adhesion strength quality according to VDI guideline (Heinke et al. 1995)

Chapter 3

Experimental Materials and Procedures

3.1 Thin Film Deposition

In the present thesis work, microwave plasma enhanced chemical vapour deposition (MPCVD) and dual ion beam system were used for synthesizing nanodiamond/DLC composite coating. MPCVD system was used to deposit nanodiamonds on titanium alloy substrate while ion beam deposition was used to deposit DLC and N-DLC films. The details of the procedures are explained in the following sections. For all the cases untreated silicon samples were used as a reference.

3.1.1 MPCVD System

Plasmionique Inc. manufactured (model number: MWPECVD 1250UOS) MPCVD reactor was used to grow nanodiamond particles on our titanium alloy substrates. The system comprises of a ASTEX–type 2.45 GHz microwave source, a vacuum chamber, a pumping system, a gas flow system and a manual control system as represented in Figure 3.1. The microwave source can be tuned to provide maximum power up to 1200 Watts. The vacuum chamber is made up of stainless steel which contains a substrate stage. The position of the substrate stage can be manually adjusted to minimize microwave power reflection. The high temperature for diamond deposition is provided by plasma heating and can be measured with a thermocouple right behind the substrate holder. Precursor gases for nanodiamond growth were CH_4 and H_2 and the flow rate of which was controlled by a multi-channel flow meter. The titanium alloy specimens were mirror polished and seeded with diamond paste manufactured by Mark V Laboratory with a particle size of 1µm for 45 min to enhance nucleation of nanodiamonds. Deposition was carried out at a microwave power of 900 Watts for a duration of 1 h.

Figure 3.1 Photograph of MPCVD System

3.1.2 Ion Beam deposition System

The thin films deposited on titanium alloy and silicon for the present research work were prepared by 4Wave ion beam system located in room 0C18, Engineering Building. The system consists of a high vacuum chamber, a pump system comprising of a mechanical and turbo pump, a rotating substrate holder which can be inclined from 0^{o} to 90^{o}, a six target assembly, sputtering targets, and two End-Hall (EH) low energy sources as shown in Figure 3.2. Figure 3.3 shows a picture of the ion beam deposition system used for deposition of DLC.

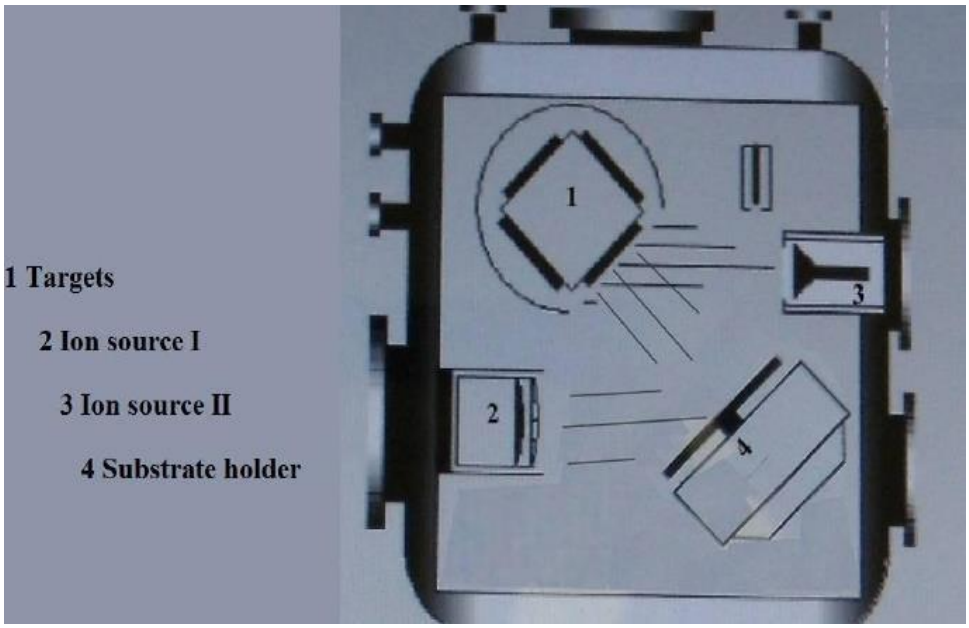

Figure 3.2 Schematic of ion beam deposition system (Zhang 2012)

The ion beam deposition system used in our experiments is capable of operating with only one source or dual sources at the same time. The system can be used to deposit DLC thin films either by direct EH ion beam source or by using ion beam assisted sputtering deposition. Hydrogen free DLC can be deposited using sputtered graphite by one EH source assisted by the second EH source whereas hydrogenated DLC films can be deposited using direct EH ion beam with methane as the precursor gas.

Figure 3.3 4 Wave ion beam deposition system

In the present thesis work, direct ion beam deposition was used to deposit DLC and N-DLC films on titanium alloy and silicon substrates with average thickness of the coatings ranging from 450 nm to 500 nm. The silicon specimens were mirror polished P-type with an average thickness of 525 µm. Titanium alloy samples used were annealed biomedical grade Ti-6Al-4V signifying an alloyed titanium product with 6 % Aluminium and 4% Vanadium. Each of the samples were cut into pieces with a dimension of 1 mm × 1 mm. Titanium alloy samples were polished with 500 µm silicon carbide paper followed by 9 µm , 3 µm and 1µm diamond polishing. The precursor gases used were a mixture of argon (Ar), methane (CH_4) and nitrogen N_2. The films were synthesized with a mean ion beam energy in the range of 65 eV to 75 eV and a beam current of 2 A. $CH_4$and Ar gas flow rates were maintained at 8sccm and 12 sccm respectively. In case of nitrogen doped DLC, three different nitrogen flow rates were used (1 sccm, 2 sccm and 3 sccm) to synthesize films with different concentration of nitrogen. In all cases, the deposition was carried out with no extra heat was supplied to the substrate. The substrate temperature can be safely assumed to be a little bit higher than room temperature because of energetic ion bombardment. The substrate holder was

inclined at an angle of 45° to the incident ion beam while the working pressure was maintained at 6×10^{-4} torr. Table 3.1 summarizes the deposition parameters for both substrates.

Table 3.1 Ion Beam Deposition Parameters for DLC and N-DLC thin films

Samples	Working Pressure (x 10^{-4} torr)	Gas Flow Ratio ($Ar/CH_4/N_2$)	Energy (eV)
ND/DLC	6	12 / 8 /0	80-85
ND/N-DLC 1	8	12 / 8 / 1	78- 80
ND/N-DLC 2	8	12 / 8 / 2	75-77
ND/N-DLC 3	8	12 / 8 / 3	75-77
ND/N-DLC 6	9	12 / 8 / 6	70-72

3.2 Chemical and Structural Characterization

Raman spectra for the samples acquired using a Reinshaw 2000 Raman system located at Saskatchewan Structural Science Center (SSSC), University of Saskatchewan. The system was operated at 514.5 nm wavelength Ar ion laser with a spot size of approximately 2μm. Five different spots were analyzed for each coated samples with the exposure time for each measurement maintained at 30s. Figure 3.4 shows the Raman spectroscope used.

Figure 3.4 Reinshaw 2000 Raman spectroscope

X-Ray photoelectron spectroscopy (XPS) measurements were performed at the Canadian Light source (CLS), University of Saskatchewan to study the composition and bonding states of the deposited films. The measurements were carried out with the help of CLS scientist Dr. Ronny Saturto. The spot size for the measurements were 3 mm^2 and samples were scanned for 5 mins. The reproducibility was ensured by scanning each specimen for 5 times. The as received data was analyzed using the Origin 9.0 software and background was removed by Shirley background removal. Near edge X ray absorption fine structure spectroscopy (NEXAFS) measurements were performed using the Spherical grating monochromator (SGM) beamline in CLS. NEXFAS studies were conducted in both total electron yield mode (TEY) and fluorescence yield mode (FLY). TEY mode is surface sensitive while FLY mode is more bulk sensitive. C K-edge for the samples were obtained in the energy window range of 280 eV to 320 eV. NEXFAS data were collected with the help of Dr. Yongfeng Hu.

3.3 Surface Morphology

Zygo NewView 8000 optical profilometer located in room OC19 , Engineering building, at University Of Saskatchewan was used to study the surface topography and film thickness while

Joel JSM -6010LV scanning electron microscope (SEM) was used to study the surface morphology after the wear and corrosion testing. The SEM was also used to study the diamond deposited titanium alloys to understand the distribution of nanodiamond particles on the substrate. Figure 3.5 and Figure 3.6 shows the pictures of the optical profilometer and the SEM respectively.

Figure 3.5 Picture of Zygo NewView Optical profilometer

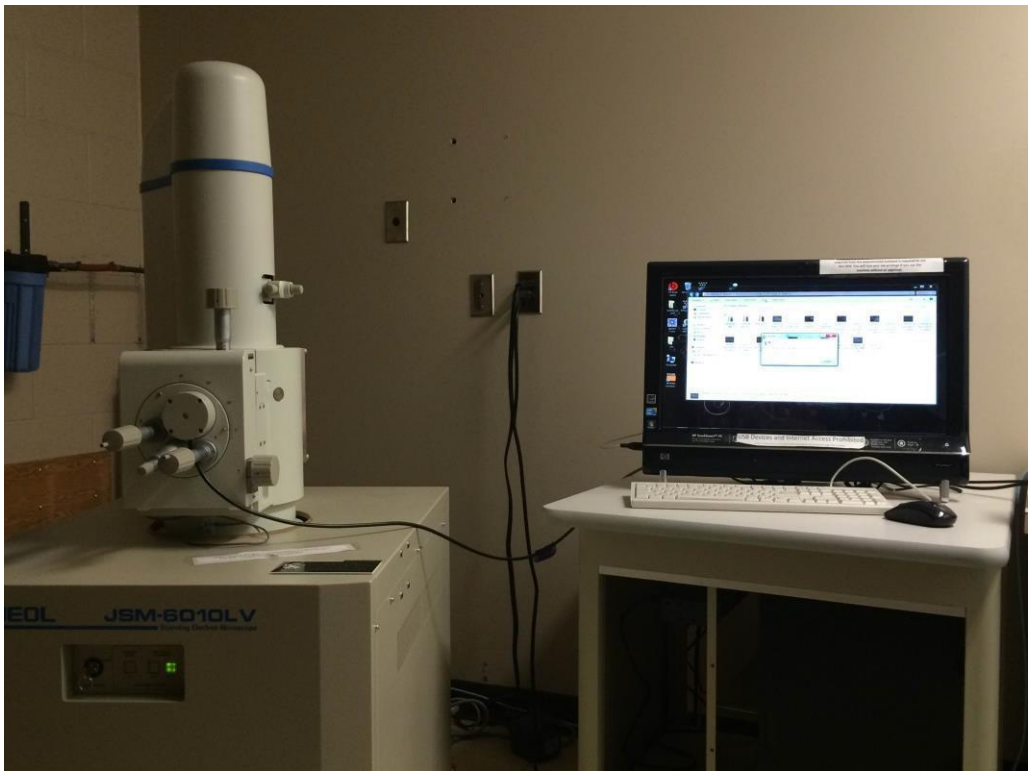

Figure 3.6 Picture of JOEL JSM 6010 LV Scanning electron microscopy

3.4 Mechanical testing

Mechanical properties of the coatings were analyzed by nano-indentation tests using a Universal Mechanical Tester (UMT) located in Room 1B22, Engineering Building. A 100 nm Berkovich indenter tip was used for the testing. The indenter tip was normal to the sample surface and driven into the sample by applying an increasing load up to a preset value. The load then gradually decreased to a point where complete or partial relaxation of the specimen has occurred. The load and displacement were continuously tracked throughout the whole process and corresponding film hardness and Young's modulus were calculated by inbuilt software based on Oliver and Pharr method (Oliver & Pharr, 1992). In the present work, nine different spots were randomly chosen for each sample to ensure the reproducibility of the hardness data and loads of 2 mN, 1 mN and 0.5 mN were used. The loads were chosen depending on the thickness of the coatings as indentation depths should be less than 15% of the coating thickness to avoid any effect from the substrate. The

indentation depths on the coatings were calculated by the software. Figure 3.7 shows the picture of nanoindentation system.

Figure 3.7 Picture of Universal Mechanical Tester

The adhesion of the coatings were evaluated by Rockwell C indentation tests. A standard load of 1497 N was used. Indents were made on three different areas for each sample. The areas around the indents were then observed using the SEM. A coating with better adhesion shows less spallation and damage, thus giving a qualitative evaluation of coating adhesion.

3.5 Corrosion Testing

Tafel polarization and electrochemical impedance spectroscopy (EIS) tests were conducted on titanium coated specimen using Gamry series G^{TM} 750 potentiostat. The tests were performed in 0.89 wt % NaCl solution in deionized water. 0.89 wt % NaCl (simulated body conditions) was used to test the corrosion resistance of the coatings, similar to the conditions used by many past researchers. For the experiments, an electrochemical cell of three electrode type was used. The

coated titanium alloy specimens were served as working electrode, the counter electrode was a pure graphite sheet while a saturated colomel electrode (SCE) was used as the reference electrode. A picture of a similar kind of Gamry potentiostat is shown in Figure 3.8.

Figure 3.8 Picture of Gamry Potentiostat

For Tafel polarization tests, the specimens were immersed in the 0.89% NaCl solution for 10 minutes for electrode stabilization prior to running the experiment. The open circuit potential (OCP) was continuously monitored and recorded during the period of electrode stabilization. The scanning range from -1.5V to +1.5 V while the scanning rate was 2 mV/sec. Bare titanium alloys, ND/ DLC coated titanium alloys and ND/N-DLC coated Ti alloys with 1 sccm nitrogen were evaluated for corrosion resistance. The exposed area for the working electrode (test samples) were 0.81cm^2. The corrosion potential (E_{corr}) and corrosion current (I_{corr}) were recorded for determining the corrosion resistance of the coatings.

Electrochemical impedance spectroscopy test was carried out for N-DLC coated specimens with 1 sccm, 2 sccm and 3 sccm nitrogen flow rate in the 0.89 wt % NaCl solution with a scan range from 10^5 Hz to 10^{-3} Hz. The specimens were immersed for 1 hour prior to the start of the test while the OCP (open circuit potential) was monitored. Bode plot for all the specimens were analyzed to evaluate the protective efficiency of the coatings. Three specimen were tested for each sample to ensure reproducibility of results.

3.6 Tribological Characterization:

Friction and wear tests were performed using Universal Mechanical Tester (UMT) at the department of Mechanical Engineering, University of Saskatchewan. Ball-on-disk configuration in a linear mode with a wear track length of 2 mm was used for the testing. The testing was carried out at ambient conditions of 25^0C with 40% relative humidity and run for 1000 cycles. For each of the tests, Ultra high molecular weight polyethylene (UHMPWE) and stainless steel balls were used respectively. A constant load of 4N was used for UHMPWE balls and 1N for stainless steel balls.

Chapter 4

Results and Discussion

This chapter is divided into two parts. Section 4.1 focuses on the adhesion of DLC based coatings. In this section studies are on the DLC, ND/DLC, and ND/NDLC coated titanium alloys. It focuses on addressing the effect of pre-deposited nanodiamond particles and nitrogen doping on the adhesion. Section 4.2 reports the electrochemical and tribological properties of the nitrogen doped DLC with different nitrogen contents.

4.1 Enhancement of Adhesion and Corrosion Resistance of diamond like carbon thin films on Ti-6Al- 4V alloy with nitrogen doping and incorporation of nanodiamond particles

Because of its high specific strength, good toughness, good biocompatibility and relatively good corrosion resistance to other common metals, Titanium and its alloys have been found widespread industrial applications in aerospace, biomedical, chemical engineering, and marine (Boyer, 1996; Budinski, 1991; Rack & Qazi, 2006; Yamada, 1996). However, extended applications of titanium and its alloys are severely limited in most cases due to their poor tribological properties and long term corrosion failures. Diamond-like-carbon (DLC) has high hardness, low wear rates and high corrosion resistance and thus can be serve as a potential candidate to enhance the surface properties of titanium alloy for their engineering applications (Erdemir & Donnet, 2006; Grill, 1993).

However, as described in section 2.2.4, DLC thin films have high amount of residual stresses due to the bombardment of energetic particles during the synthesis. High residual stresses in films causes poor adhesion to the metallic substrates (Grill 1993; Robertson 2002; Zhang et al. 2013). Researches in the past decades had adopted various techniques to minimize the stress in DLC and improve its adhesion to the substrates. This includes using of single buffer interlayer (Si,Cr)(Costa

et al., 2011; Kim et al., 2005); functionally graded interlayers (Ti/TiC/DLC, Ti/TiN/DLC, Ti/TiN/TiNC/DLC)(Choy & Felix, 2000); surface plasma treatment or etching with Ar; chemical structure modification by various metallic(Ti, Cr, Ni) and non –metallic doping (N, F, Br, B)(Anita et al., 2004; Singh et al., 2006).

In the present work, a novel technique was employed to reduce the stress and to increase the adhesion of DLC films to Ti-6Al-4V substrate, namely, incorporation of both nanodiamond particles and nitrogen into DLC films. The details of the deposition techniques were described in Chapter 3. The results and discussion are presented in this section.

4.1.1 Chemical Characterization:

4.1.1.1 Raman Spectra and SEM of Diamond nanoparticles on Ti-6Al-4V

Figure 4.1 demontrates the Raman spectrum of the samples after diamond deposition. The presence of dimond characteristic peak at 1334 cm^{-1} indicates the formation of diamond nanoparticles on the surface while the peak at 1600 cm^{-1} illustrates the presence of graphitic carbon simultaneously on the surface. Figure 4.2 shows a typical SEM image of the nanodiamond particles deposited on the highly polished titanium alloy substrate. It can be clearly seen that nanodiamond particles have been grown over the entire substrate.

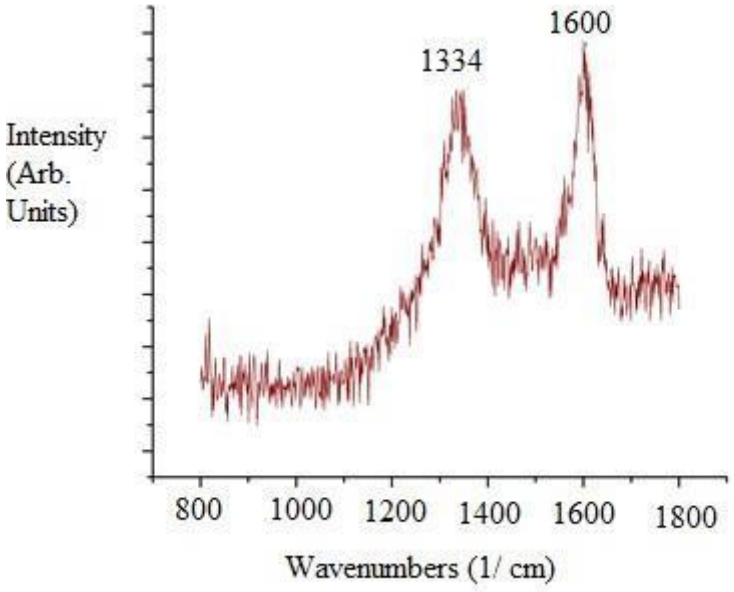

Figure 4.1 Raman Spectrum of nanodiamonds on the titanium Alloy

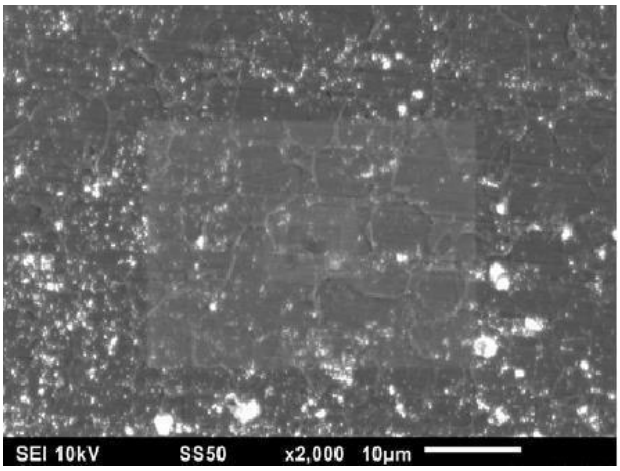

Figure 4.2 SEM image of nanodiamonds grown on the titanium alloy

4.1.1.2 Raman Spectra of DLC and N-DLC

The Raman spectra obtained from deposited DLC and N-DLC specimens are shown in Figure 4.3. All the spectra show characteristic peaks of DLC, the disordered D peak at around 1360 cm^{-1} and

the graphitic G peak at around 1575 cm^{-1} . The broad nature of the peaks shows the amorphous nature of the coatings. The relative intensities of I_D/I_G gives an estimate of the sp^2/sp^3 bonding ratio in DLC. Increase in the ratio implies the increase of sp^2 bonding percentage in the coating. DLC and N-DLC deposited on silicon substrates shows I_D/I_G as 0.36 and 0.41, respectively. I_D/I_G ratio is noted to be 0.31 and 0.67 for DLC and N-DLC on Titanium alloys, respecitively. The position of G- peak shifted from 1537 cm^{-1} to 1555 cm^{-1} on Silicon and from 1538 cm^{-1} to 1567 cm^{-1} on the alloy substrate for N doped DLC samples. This indicates that N doping causes slight increase in sp^2 bonding in the coating.

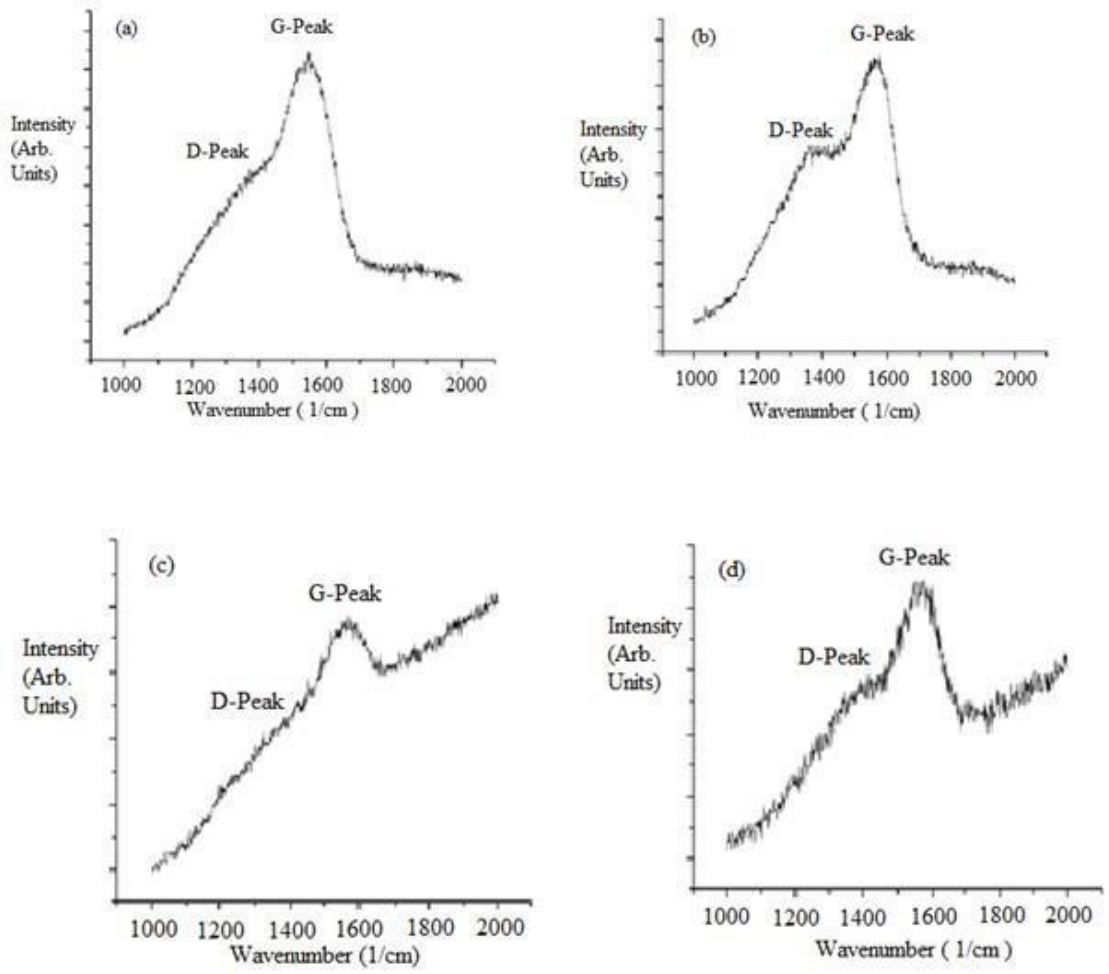

Figure 4.3 Raman Spectra of (a) DLC on Silicon, (b) N-DLC on silicon, (c) ND/DLC on titanium alloy, and (d) ND/N-DLC on titanium alloy

4.1.1.3 X-Ray Absorbtion Spectroscopy

Carbon K edge spectra of the samples are shown in figures 4.4 and 4.5. Figure. 4.4 shows the spectra obtained in TEY(total electron yield) mode while figure.4.5 describes the measurement results in FLY (flouroscence yield) mode. There are three peaks, 285.1 eV , 288.0 eV and 292.0 eV, appearing in all the spectra in Figure 4.4 .The peak around 285.1 eV is contributed by electronic transition of C1s->π^* for sp^2 C=C bonds. The peak around 288 eV is due to the presence of sp^3C-H bonds which are justified as surface dangling bonds of carbon passivated by hydrogen in the coatings. The peak at 292 eV can be attributed to the sp^3 C-C σ^* bonds (McCann et al., 2005). An extremely low intensity peak appears at around 287.5 eV in the spectra, which can be attributed to C=O π^* bonding. This C=O bonding on the surface could be due to the reaction between carbon and oxygen after deposition. The spectra obtained in TEY mode are surface sensitive whereas the information in FLY mode is from both the surface and inner layers. TEY spectra shows relatively stronger sp^3 peaks, indicating higher content of sp^3 bonds on the surface. This is probably attributed to the higher content of C-H bonds on the surface. N-DLC shows similar spectra as DLC in this study, indicating that low nitrogen doped DLC doesn't significantly change the bonding characteristics compared to pure DLC. The spectra in FLY mode shown in Figure.4.5 are mainly composed of two characteristics peaks (Casiraghi et al. 2005) around 285.1 eV and 292.0 eV with no peaks around 288.0 eV and 287.5 eV indicating that at the inner part of the coating consists mainly of sp^2 C=C and sp^3 C-C bonding. The missing of oxide peak at 287.5eV indicates that C=O only forms at the surface of the samples, probably due to surface contamination after deposition.

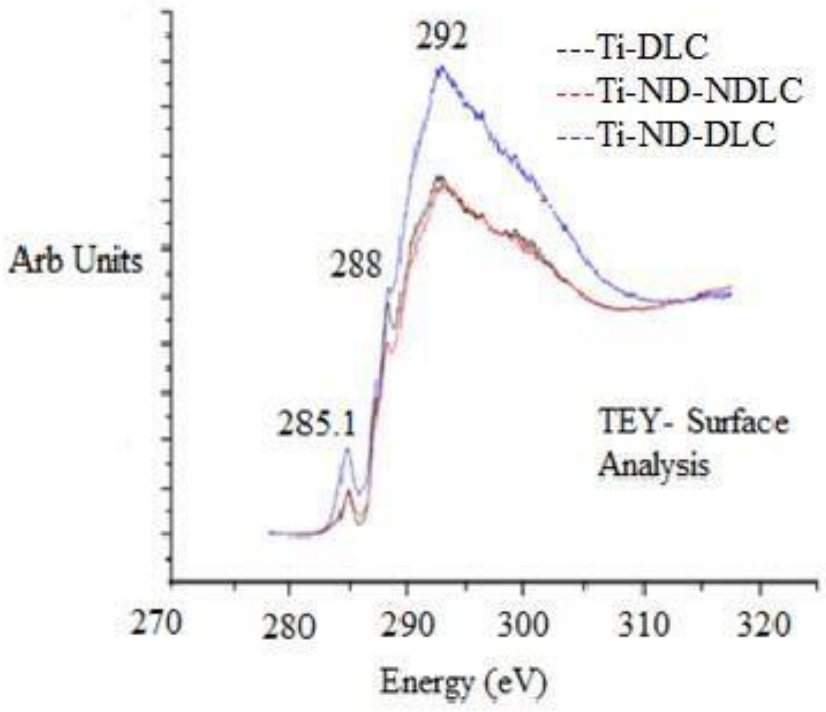

Figure 4.4 C-K edge XAS in Total Electron Yield (TEY) mode

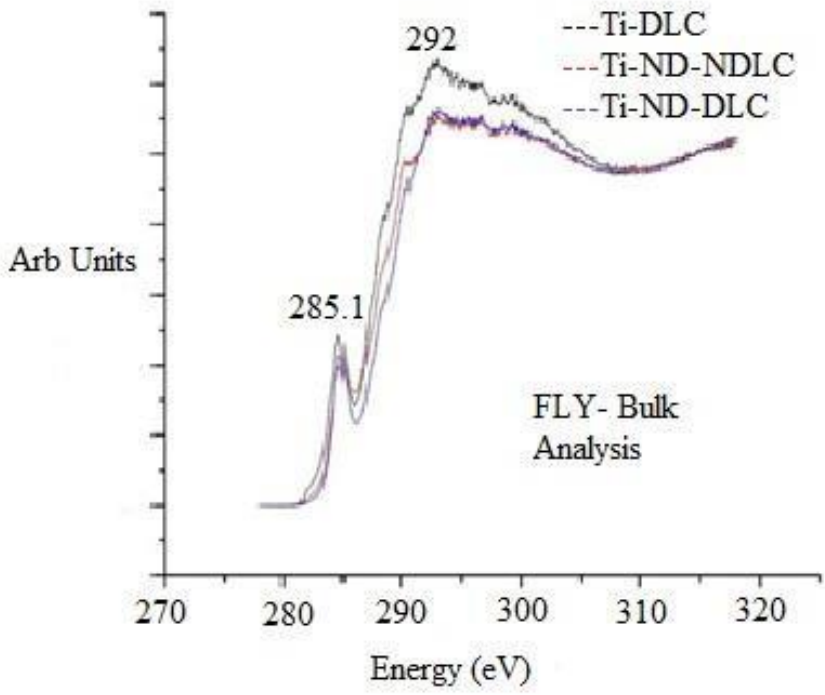

Figure 4.5 C-K edge XAS in Flourescence Yield (FLY) mode

4.1.2 Surface Morphology

SEM was used to study the surface morphology of the coatings on titanium alloy with and without nanodiamond particles deposition. The SEM observation of the samples shows that DLC on alloy substrates with pre-deposited nanodiamond particles exhibited smooth and uniform structure as represented in Figure 4.6 (b) whereas DLC deposited directly on alloy substrate shows poor adhesion as delamination and buckling of films were observed, as shown in Figure 4.6 (a). Those results show that pre-deposition of diamond nanoparticles can improve the adhesion of DLC on the Ti alloys.

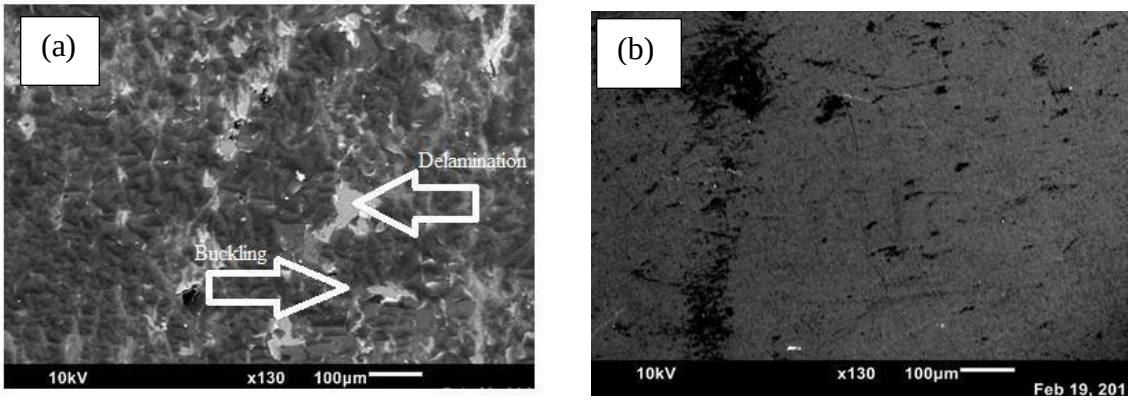

Figure 4.6 SEM image comparison of (a) DLC on titanium alloys and, (b) ND-DLC on titanium

4.1.3 Surface Tomography

Surface tomographic images of titanium alloys, nanodiamond particles, DLC coated and N-DLC coated alloys using optical profilometer are shown in Figure 4.7. The roughness of different samples are summarized in Table 4.1.1. Alloy substrates were well polished and have an average roughness of 18.5 nm. With the deposition of the diamond-nanoparticles, the roughness value decreases to 10.6 nm. This can be attributed to the uniform deposition of diamond nanoparticles at grooves in the substrates (please see Figure.4.2). However, deposition of DLC on nanodiamond particles increases surface roughness. This is probably because of the presence of sp^2 C-H dangling bonds on the surface in hydrogented DLC (Srinivasan et al. 2012).

Table 4.1 Surface Roughness of Ti alloys and coated alloys

Samples	RMS roughness(nm)	Average Rougness(nm)
Bare Ti alloy	23.7 ± 2.0	18.5 ± 2.0
Nano-Diamonds on Ti alloy	17.3 ± 3.0	10.6 ± 4.0
ND-DLC on Ti alloy	38.4 ± 3.0	30.5 ± 2.0
ND-N-DLC on Ti alloy	21.5 ± 2.0	16.4 ± 1.0

Nitrogen doped DLC has much lower roughness than DLC, indicating N-doping can reduce roughness, which is probably due to the decrease of C-H dangling bonds on the surface (Tang et al. 2011). These results are consistent with our previous work for DLC and N-DLC on PTFE (Srinivasan et al. 2012).

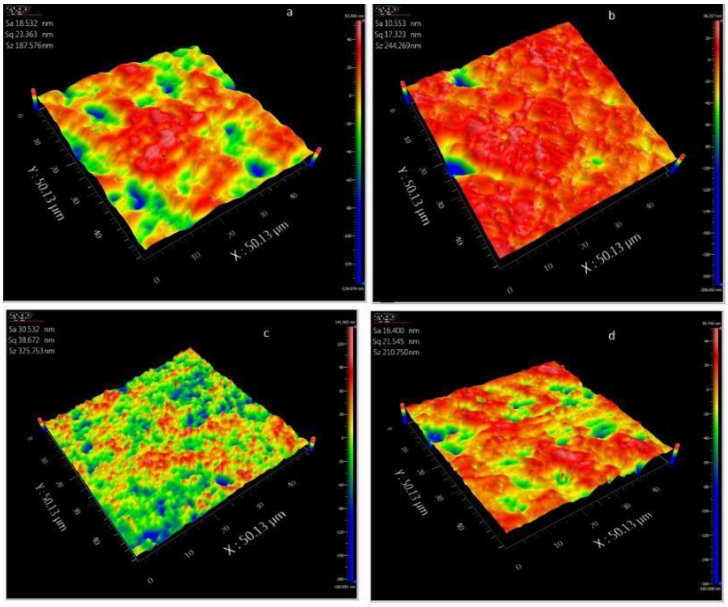

Figure 4.7 Profilometer tomography images a: polished titanium alloy, (b) Nanodiamonds on titanium alloy, (c) DLC on nanodiamond predeposited Ti alloys, (d) N-DLC on nanodiamond predepsoited Ti alloy

4.1.4 Adhesion

Rockwell C indentation tests were performed on the samples to estimate the adhesion of DLC and N-DLC on Ti-6Al-4V substrate. The indentation load used for the tests was 1470N (Heinke et al., 1995). Figure 4.1.8 shows the SEM images of the samples after Rockwell C testing performed on DLC, ND-DLC and ND-N-DLC coatings on Ti-6Al-4V. The cracking and spallation around the indentation area due to the high loading can give us an estimate of the adhesion of coating to the substrate. DLC deposited on bare titanium alloy, as shown in Figure 4.8(a), shows severe damage and delamination, indicating poor adhesion of DLC on Ti alloys. Figure 4.8(b) shows some cracks and light spallation of film while Figure 4.8(c) shows microcracks and little delamination of film. The results indicate that both nanodiamond and nitrogen incorporation can increase DLC adhesion to Ti alloys. The trend of increased adhesion from Figure 4.8(a) to Figures 4.8(c) can be explained by Griffith's law (Mosaner et al. 2003):

$$\frac{\sigma^2 h}{2E} \leq 2\gamma \qquad (4.1)$$

where σ in the equation represents the compressive stress in the film which is a direct function of the elastic energy stored in a coating of certain thickness, *h* represents the thickness, *E is* the elastic modulus and γ represents the surface fracture energy. The growth due to the bombardment of high energetic particles tends to form high fraction of sp^3 C-C bonds and also stretch the substrate. Thus the substrate has profound effect in contributing towards compressive stress in the coating resulting in shear stress between the interface (Mosaner et al. 2003). The interface thus serves as a critical region for adhesion of coatings. High amount of compresssive stress contributes towards high elastic energy in a coating and it fails when elatic energy reaches a critical value for substrate coating interface. According to the above equation, coating fails when the left hand side of the above equation is equal to the right hand side. In the case of DLC deposited on Ti alloys, the film has high amount of residual stress, thus the film delaminated under the load and showed lowest adhesion. The incorporation of nanodiamonds into the film enhances adhesion by increasing mechanical interlocking between Ti alloy substrate and DLC film. The best adhesion is observed for incorporation of both nitrogen and nanodiamonds into DLC films. This might be attributed to

the relief of stress σ by lowering the elastic strain energy because of the increase of sp^2 bond

fractions by nitrogen doping combining with the increase of surface energy by incorporation of nanodiamond particles. Similar increase in the sp^2 content with nitrogen doping were reported by Sullivan and co-workers (Sullivan et al. 1997).

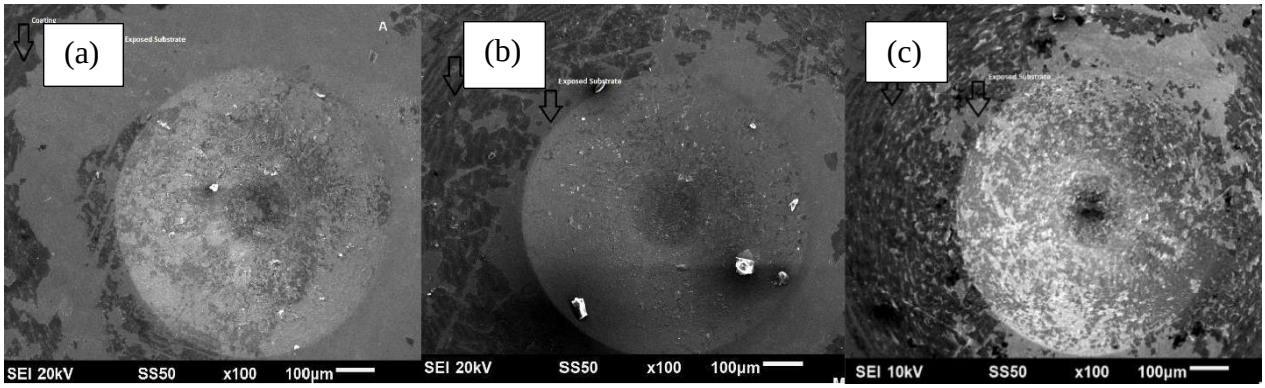

Figure 4.8 SEM images after Rockwell C indentation,(a) DLC on bare Ti alloy, (b) ND-DLC on Ti alloy and(c) ND-N-DLC on Ti alloy

4.1.5 Mechanical Properties

The hardness and Young's modulus of the coatings were calculated based on nano-indentationon nine different locations for each sample. The hardness and Young's modulus of DLC was around 11±0.5 GPa and 98±4 GPa, respectively. For N-DLC, the average hardness decreases slightly to about 9±0.4 GPa while the Young's modulus was calculated to be around 95± 5 GPa. It is also noted that the DLC films deposited in the present research show relatively lower hardness, this is probably because of the use of low energy ions for the synthesis. Nitrogen doped DLC has slightly lower hardness which is probably due to its lower sp^3 C-C bonding concentration as shown in Figure 4.3.

4.1.6 Corrosion Testing

The potentidynamic polarization curves of the samples after corrosion tests in 0.89% NaCl are shown in Figure 4.9.

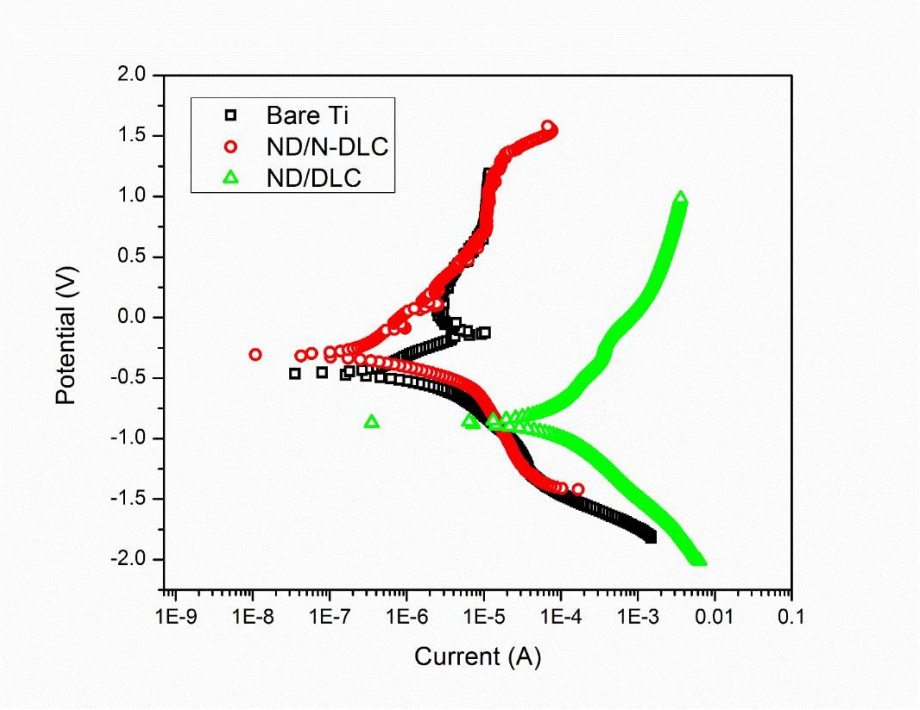

Figure 4.9 Potentiodynamic polarization curves of films measured in 0.89% NaCl solution

The polarization curves show two sections. The Cathodic polarization generally refers to the hydrogen evolution through water reduction, whereas the anodic polarization signifies the dissolution of the tested material. The important parameters for determining the corrosion resistance of the coating is the corrosion potential E_{corr} and corrosion current density I_{corr}. These critical parameters could be obtained by applying Tafel extrapolation technique to the polarization curve. Based on the results of the polarization curves as shown in Figure 4.9, it can be seen that both nitrogen doping and nano-diamond particle incorporation increase the corrosion resistance of DLC coatings. The corrosion potential for ND-N-DLC-is 2.3x 10^{-9} A/cm^2, lower than that of bare Ti alloys which showed a current density of 5.2x 10^{-9} A/cm^2. ND/DLC films show increased

current density of 6.2x 10^{-5} A/cm^2, indicating poor corrosion resistance. Table 4.2 shows the corrosion potential and corrosion current density of the samples.

Table 4.2 Corrosion Data after Tafel fitting of the Polarization curves in 0.89% NaCl

Samples	E_{corr}	I_{corr}
Bare Titanium alloy	-0.48V± 0.04	(5.2 ± 0.4) x10^{-9} A/cm^2
DLC on ND Titanium alloy	-0.81V±0.10	(6.2 ± 1.2) x 10^{-5}A/cm^2
N-DLC on ND Titanium alloy	-0.32V±0.04	(2.3 ± 0.3) x 10^{-9} A/cm^2

The poor corrosion resistance of ND/DLC films could be due to several reasons. Although DLC is electrochemically nobler than most of the materials but factors such as uniformity of the coating, defects, film structure, surface roughness and interfacial states play a vital role in determining the corrosion resistance of DLC films. Corrosion in DLC generally initiates at points of imperfections, large compositional inhomogenity and regions of high stresses (Wu et al. 2010).

ND-DLC fims show higher surface roughness compared to both ND/N-DLC and bare Ti alloys. This results in larger exposed surface area to the electrolyte. XAS spectra in Figure 4.4 shows relatively higher amount of C-H bonding in the case of ND-DLC compared to ND-N-DLC. The presence of such bonds could give rise to atomic scale voids (Y. Tang et al. 2011). Such voids induces micro-cracks and minor pinholes in DLC, allowing a free path from the electrolyte to the coating substrate interface. Local galvanic corrosion at exposed coating/substrate interface may further accelerate corrosion and decrease the corrosion resistance (Sullivan et al. 1997, Wu et al. 2010). ND/N-DLC coatings have lower surface roughness thus smaller surface area exposing to the electrolyte. Their better adhesion, reduced extrinsic stress (due to nitrogen doping) and lower intrinsic stress induced defects and cracks enhance corrosion resistance.

4.2 Effect of nitrogen content on electrochemical and tribological properties of ND/N-DLC films on Ti-6Al-4V substrates

The results illustrated in section 4.1 clearly show that co-incorporation of nanodiamonds and nitrogen into DLC greatly enhances the adhesion and smoothness of DLC and thus the corrosion resistance. In this section, the results of effect of nitrogen content on chemical, mechanical, tribological, and electrochemical properties of N-DLC coatings has been studied and is being presented..

4.2.1 Chemical Bonding and Structural Characterization

4.2.1.1 Raman Spectra and XPS of nanodiamonds grown by MPCVD

The Raman spectrum of the nanodiamonds deposited on polished Ti alloy samples has been shown in the previous section (Figure 4.1). The parameters used in this section for nanodiamond deposition are similar to those presented in section 4.1. And the Raman spectra of the nanodiamond showed two peaks at 1332 cm^{-1} and at 1600 cm^{-1}, respectively, similar to the Raman spectra presented in Section 4.1. XPS was further used to verify the diamond nature of the nanoparticles. The XPS spectrum of nanodiamonds on the titanium alloy is presented in Figure 4.10. The spectrum shows two peaks at 281.7 eV and 284.6 eV. The peak around 284.6 eV is attributed to carbon to carbon bonds and the peak approximately at 281.7 eV represents titanium carbide peaks (Zhang & Koka, 1998). The results indicate that during diamond deposition the titanium in the substrate acts with carbon to form a carbide phase. The titanium carbide phase at the interface facilitates chemical bonding with carbon to enhance adhesion of DLC and helps in reducing the mismatch between the substrate and the coating forming a gradual compositional and property transition.

SEM image of the nanodiamonds (one hour deposition) shown in Figure 4.11 shows uniform nanodiamond particles on titanium alloy surface.

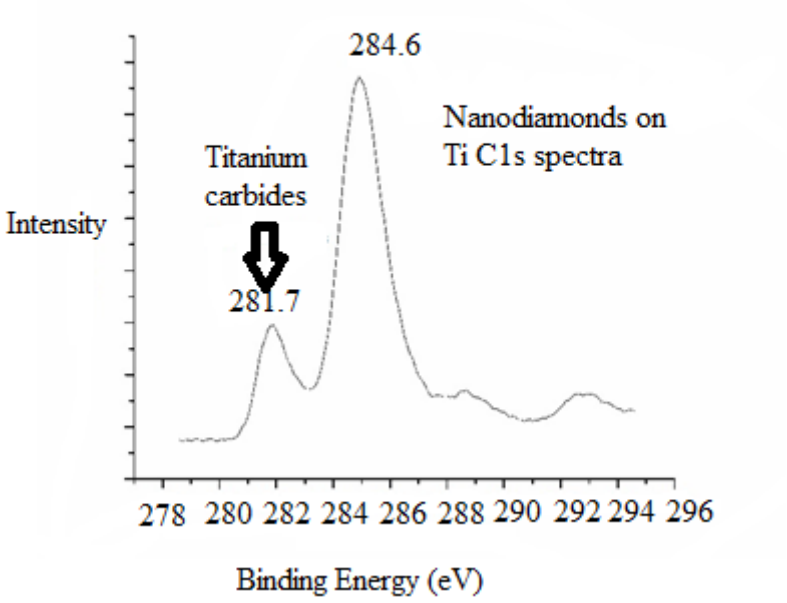

Figure 4.10 C1s XPS peak for nanodiamonds on titanium alloy

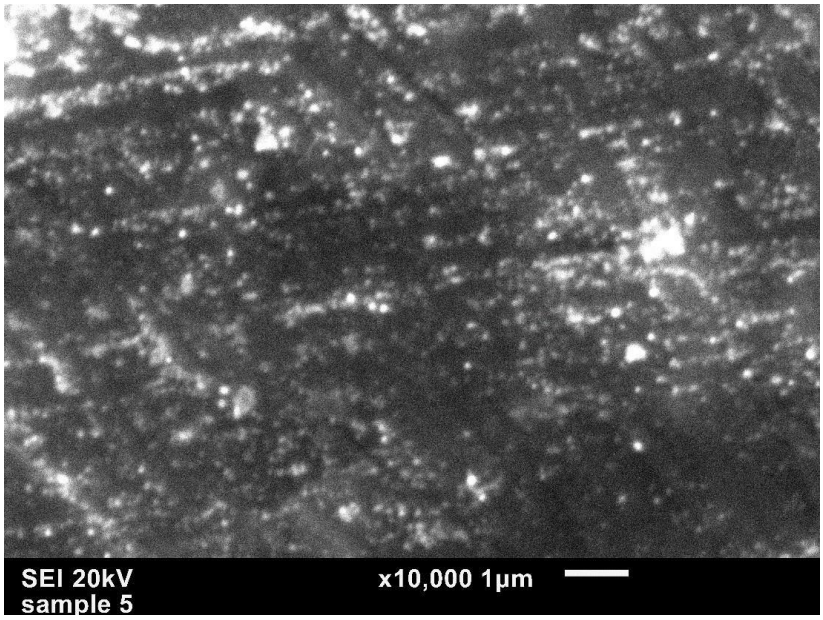

Figure 4.11 SEM image of nanodiamonds grown on titanium alloy

4.2.1.2 XPS of nitrogen doped DLC films

The N/C atomic ratio can be obtained from the ratios of the areas of N1s and C 1s peaks considering atomic sensitivity factor. It shows that there is an increase in nitrogen content with increasing nitrogen flow rate. The N/C ratio increased from 0.24 to 0.42 when nitrogen flow rate increases from 1sccm to 6 sccm.

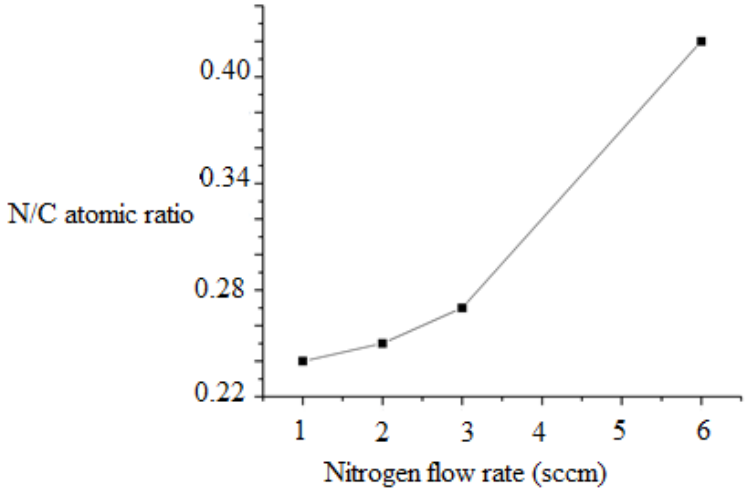

Figure 4.12 N/C atomic ratio versus nitrogen flow rate

The XPS of C1s core level spectra of N-DLCs are shown in Figures 4.13–4.16. Each peak was de-convoluted using Gaussian function and Shirley background removal. The Gaussian fitting to the XPS lines results in five different components of carbon bonding in C1s spectra. The peaks at 284.5 eV, 285.4 eV, 286.3 eV, 287.5 eV and 288.8 eV are attributed to C=C, C-C, C=N, C-N and C-O bonds, respectively (Seker et al. 2014; Hayashi et al. 2001). C=N/C-N were calculated according to their corresponding peak area ratios after fitting. Figure 4.17 shows the variation of

C=N/C-N with nitrogen flow rate. It can be clearly seen that with increasing nitrogen flow rate the fraction of C=N with respect to C-N increases. Thus it can be stated that increase in the nitrogen content promotes more graphite like double bonded structure, which is consistent with Raman spectroscopic results presented previously (Das et al. 2003) Similar increase in C=N content for nitrogen-doped DLC was reported by other researchers (Hayashi et al., 2001; Seker et al. 2014).

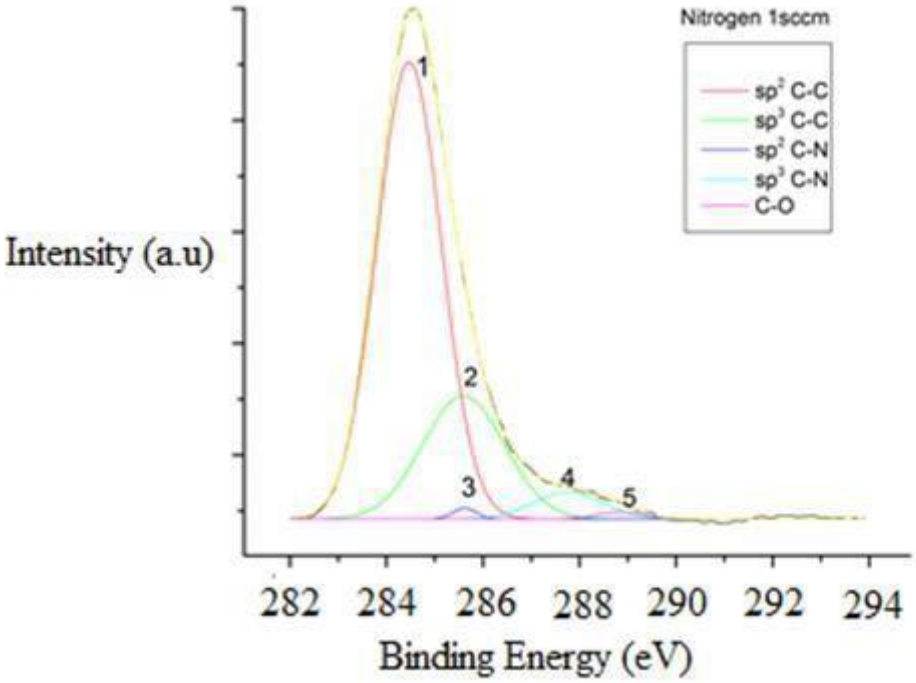

Figure 4.13 XPS C1s of N-DLC with 1 sccm nitrogen flow rate

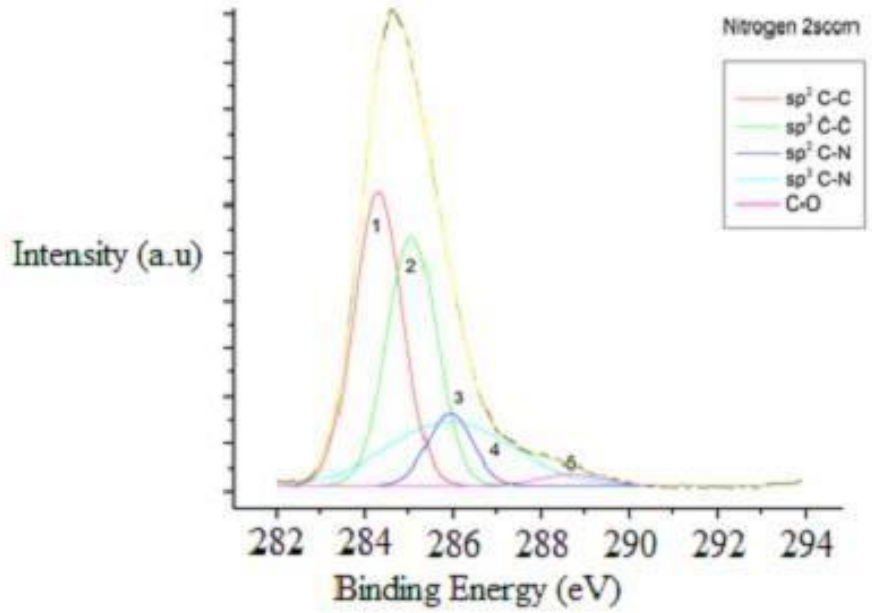

Figure 4.14 XPS C1s of N-DLC with 2 sccm nitrogen flow rate

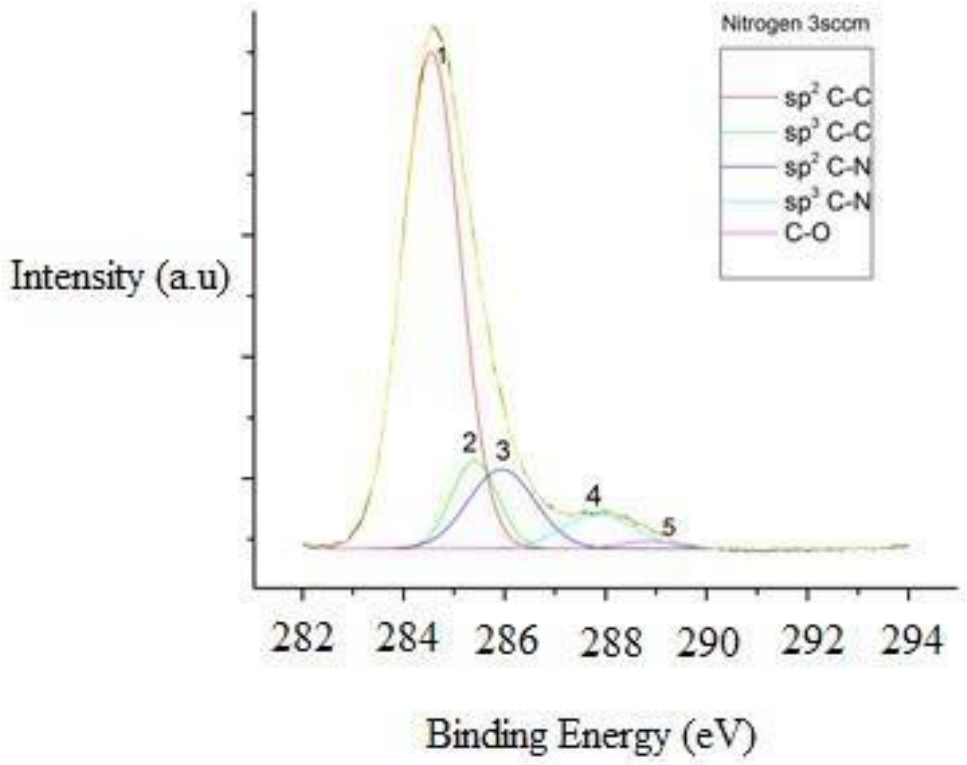

Figure 4.15 XPS C1s of N-DLC with 3 sccm nitrogen flow rate

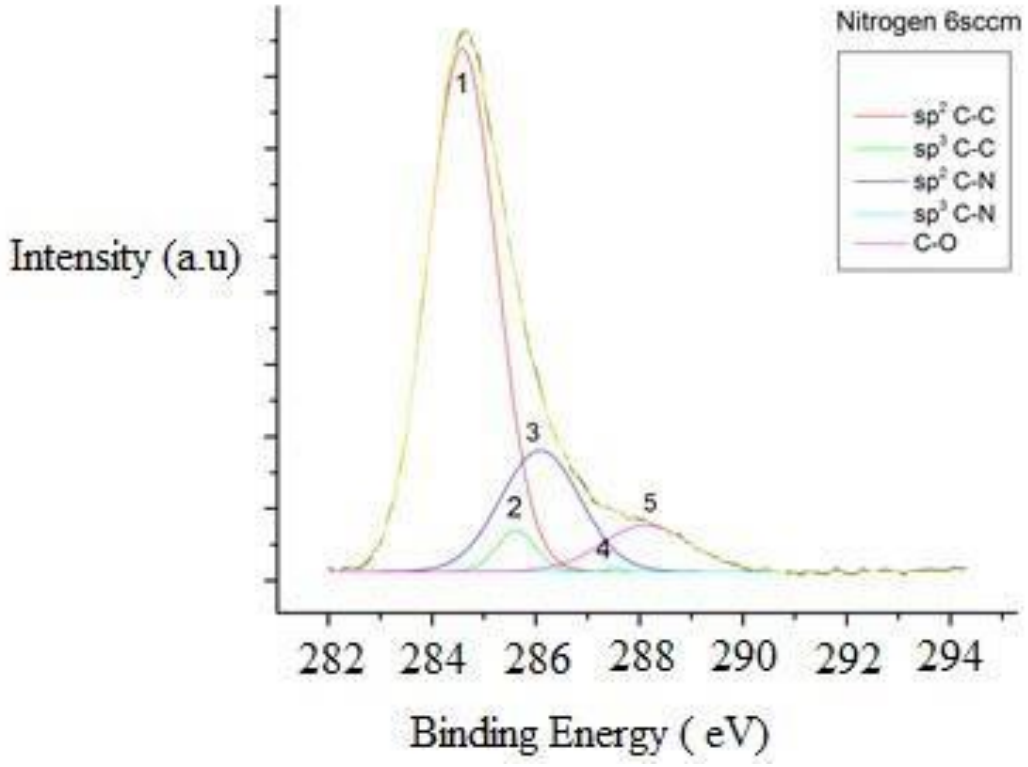

Figure 4.16 XPS C1s of N-DLC with 6 sccm nitrogen flow rate

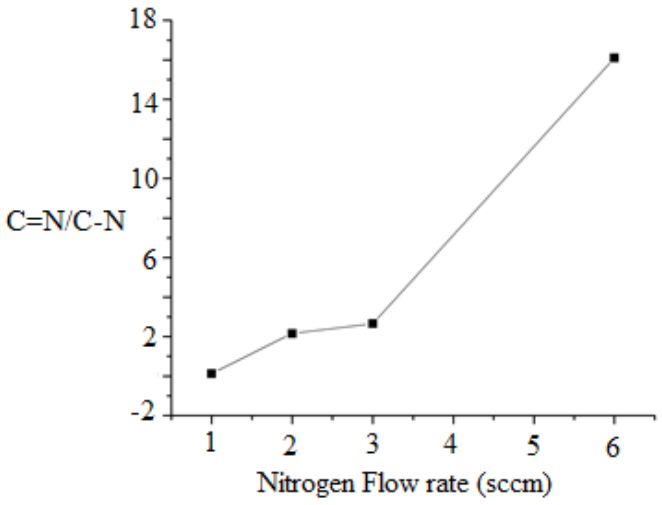

Figure 4.17 C=N/C-N ratio vs nitrogen glow rates

4.2.1.3 NEXAFS of nitrogen doped DLCs:

Nitrogen K-Edge spectra of N-DLC coatings are shown in Figure 4.18 for nitrogen flow rates of 1 sccm, 2 sccm, 3 sccm and 6 sccm. All the spectra show four prominent peaks, approximately around 399 eV, 400 eV, 401.7 eV, 408 eV marked as P_1, P_2, P_3 and P_4. An additional small peak P_N at approximately 404 eV is observed for nitrogen flow rate of 6sccm. The peaks at lower energy (P_1, P_2 and P_3) are mainly contributed by π^* peaks while the peak at higher energies, i.e, peak P_4 is mainly contributed by of σ* bonding. Several authors have assigned peak P_1, P_2 and P_3 to pyridine like nitrogen, triple bonded CN and substitutional nitrogen in graphite respectively (Roy et al. 2005, McCann et al. 2005). Other authors claim that peaks P_1 and P_2 are interrelated while the peak P_3 could be due to graphite like nitrogen substitution or bound nitrogen atoms in the films. The origin of P_2 is difficult to assign and could be due to nitrogen bonded to C with different functionalities (S. S. Roy et al. 2005). In our present investigation, the relative intensity ratio of peaks P_2 to P_3 keeps on increasing with the increase of nitrogen content. This could be possibly due to the formation of triple bonded nitrogen with carbon atoms because of increased nitrogen

content. It is interesting to note that peak P_1 decreased significantly in the sample with nitrogen flow rate of 6 sccm, which signifies that at high nitrogen concentration most of the nitrogen prefers to form triple bonded configuration or trapped nitrogen atoms in the coating rather than pyridine like structure.

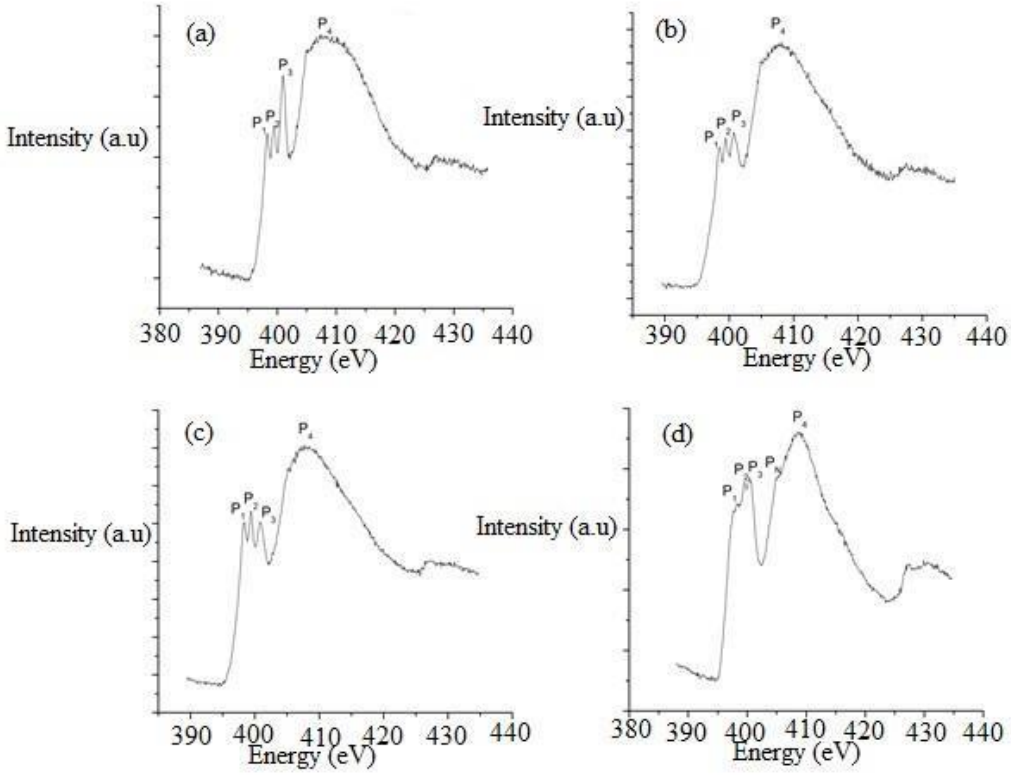

Figure 4.18 NEXAS N K-Edge Spectra of N- doped DLC (a) N flow 1sccm, (b) N flow 2sccm,(c) N flow 3 sccm, (d) N flow 6 sccm

4.2.1.4 Raman Spectra of nitrogen doped DLC

Because of the high Raman scattering cross sections of sp^2 sites (Robertson 2008), the visible Raman spectrum of DLC is dominated by the D peak and G peak of graphitic carbon bonding (sp^2 sites). G peak originates from the stretching vibration of the sp^2 sites in both chain and aromatic rings whereas the D peak is contributed by the breathing mode of the sp^2 sites in the rings (Robertson 2002). The parameters such as intensity ratio of I_D/ I_G peaks, the position and full width

of half maximum (FWHM) of the G peak of a Raman spectrum can give valuable information about the bonding structure of DLC coating (Casiraghi et al. 2005).

Figure 4.19 shows typical Raman spectra of nitrogen doped DLC prepared with different flow rates of nitrogen gas. DLC coatings with different nitrogen concentrations was prepared by changing nitrogen gas flow rate (1 sccm, 2 sccm, 3 sccm and 6 sccm, respectively) in the gas mixture. The Raman spectra were fitted by Wire software using Gaussian- Lorenztian function to obtain the intensity and position information of D peak and G peak. The G peak position shifts to higher wavenumber while I_D/I_G value shows gradual increase with the increase of nitrogen flow rate from 1sccm to 6sccm as shown in Figure 4.20. The position of the G peak is 1563 cm^{-1} ,1564 cm^{-1}, 1568 cm^{-1} and 1584 cm^{-1}, respectively, corresponding to I_D/I_G of 0.672, 0.752, 0.827 and 0.876, respectively, as nitrogen flow rate increases from 1sccm to 6sccm. The increase of I_D/I_G ratio with the increase of nitrogen concentration indicates sp^2 bonding content in DLC coating increases with the increase of nitrogen content. As the intensity of the D peak greatly depends on the breathing mode of the sp^2 sites. it can be stated that nitrogen doping promotes clustering of the sp^2 bonds into rings rather than forming chains (Zhou et al. 2015, Scharf et al. 1999, Marton et al., 2012). Similar inference can be made from the shifting of the G peak position to higher wavenumbers. The FWHM of the G peak in Raman spectra is sensitive to structural disorder which arises from bond angle and bond length disorder (Casiraghi, Ferrari, et al., 2005). In the present investigation, the FWHM of the G peak increases as nitrogen flow rate increases from 1 sccm to 3 sccm but decreases significantly with further increasing nitrogen in flow rate of 6 sccm. This indicates that with low concentrations of nitrogen there is a slight increase in structural disorder with the increase of nitrogen content due to the small clusters of sp^2 sites in the coating but high concentration of nitrogen reduces structural disorder caused by small clusters. Similar results were reported on amorphous carbon-nitride films by Ferrari et al (Ferrari et al. 2003).

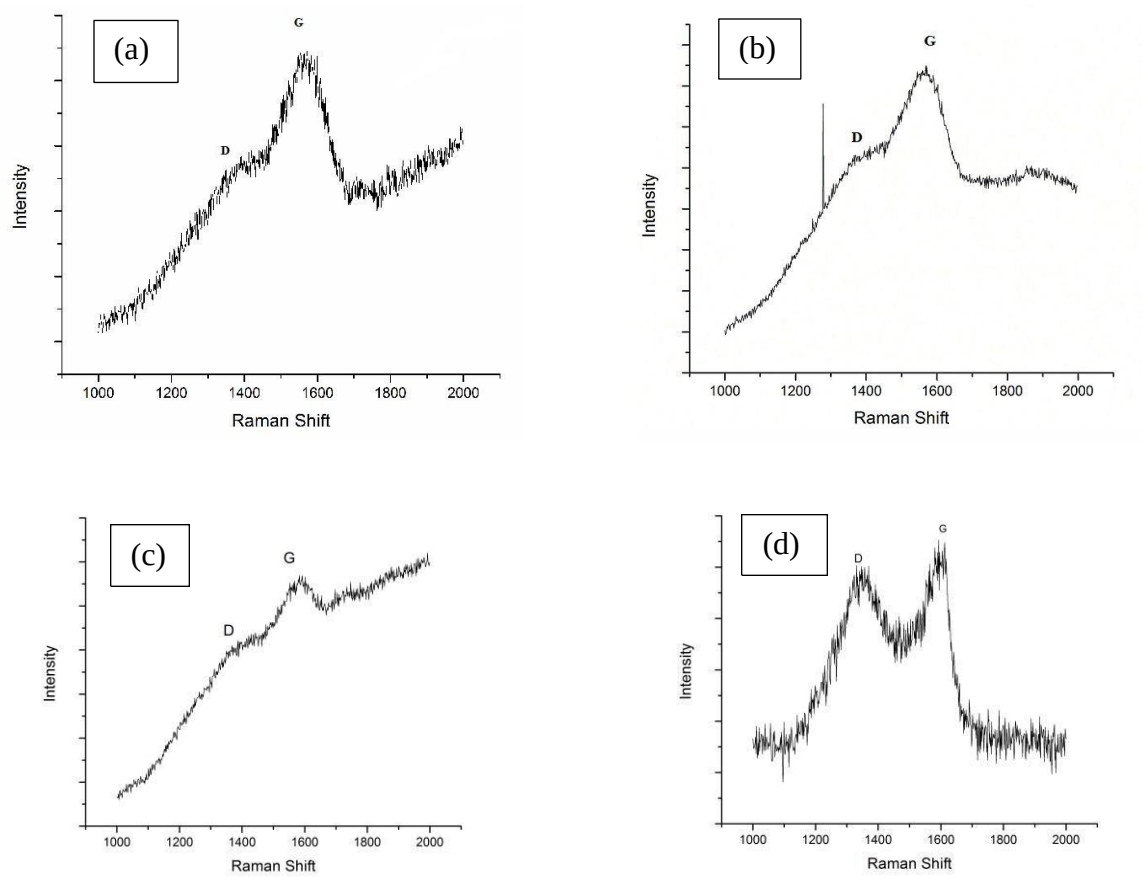

Figure 4.19 Raman Spectra of Nitrogenated DLC on nano-diamond titanium alloys showing relative change in peak intensities (a) Nitrogen 1 sccm, (b) Nitrogen 2 sccm, (c) Nitrogen 3 sccm, and (d) Nitrogen 6 sccm

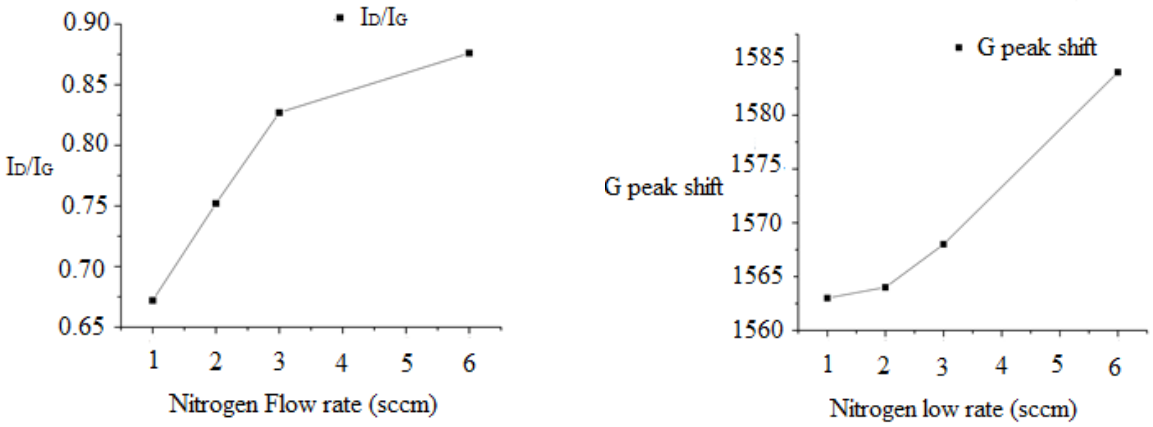

Figure 4.20 Plots of I_D/I_G and G peak shift versus the nitrogen flow rate

4.2.2 Surface topography

Optical profilometer is used to study the surface tomography of the N-DLC samples. Table 4.3 summarizes the roughness values for nitrogen doped samples with 1sccm, 2sccm, 3sccm and 6sccm respectively. The roughness of the coatings were contributed by several factors such as surface preparation, angle of ion beam incidence, energy of the ions and chemical structure. The surface roughness value increased with the increase of nitrogen concentration. Since the preparation and deposition conditions in the present study was similar, plausible explanation for increased roughness for higher nitrogen doping could be due to higher graphitic structure as indicated by XPS and Raman investigations. Similar increase in the roughness with nitrogen incorporation in the DLC structure was reported previously (Zou et al. 2009).

Table 4.3 Surface roughness of N-DLC films with optical Profilometer

Samples	Average Roughness(nm)
N-DLC 1sccm	17.9 ± 1.5
N-DLC 2sccm	22.4 ± 2.0
N-DLC 3sccm	26.8 ± 2.1
N-DLC 6sccm	32.8 ± 2.6

4.2.3 Hardness

The hardness of the coatings was evaluated by nano-indentation technique. The hardness of the N-DLC coatings gradually decreased with the increase of nitrogen concentration in the DLC coatings. N-DLC with 1sccm flow nitrogen flow rate showed an average hardness of 9.5 GPa followed by 7.8 GPa, 7.2 GPa and 5.8 GPa for flow rates of 2 sccm, 3 sccm and 6 sccm nitrogen respectively. The hardness of DLC is mainly contributed by C-C bonding networks. Films with higher concentration of sp^3 C-C bonding will have higher hardness. As XPS and Raman spectra show that higher flow rate of nitrogen results in higher N/C atomic ratio and lower concentration of sp^3 C-C bonding. Figure 4.21(a) graphically represents the variation of hardness and C=N/C-C fraction with respect to the nitrogen flow rate. C=N/C-C ratio increases from 0.02 to 6.11 when nitrogen flow rate increases from 1 sccm to 6 sccm. C=N/C-C ratio shows the degree of breaking of the C-C bonding by nitrogen addition, thus low C=N/C-C ratio of 0.02 keeps high concentration of C-C bonding and hence high hardness. Increased nitrogen concentration promotes more sp^2 sites with reduced sp^3 C-C sites and increases in I_d/I_g ratio leading to decrease in hardness as revealed in Figure 4.21(b). Decrease in hardness for nitrogen doped DLCs has been previously reported by other authors (Cheah et al., 1998; Ruijun & Hongtao, 2006).

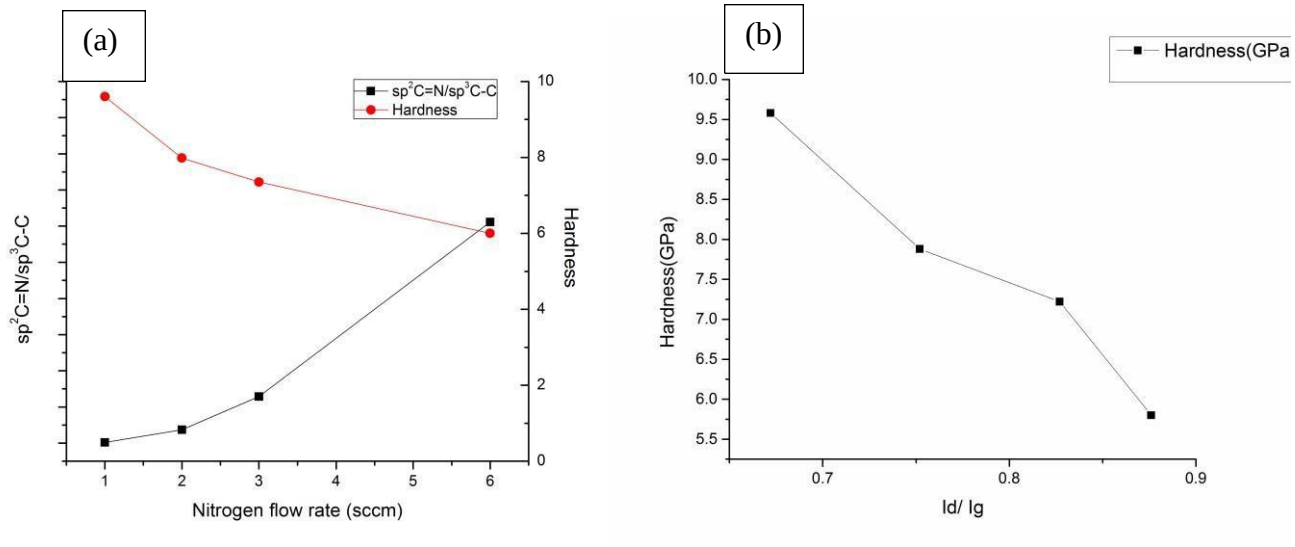

Figure 4.21 Figure showing variation of (a) Hardness and C=N/C-C bonding ratio with nitrogen flow rate, (b) Hardness against I_d/I_g ratio

4.2.4 Adhesion

Rockwell C adhesion testing was performed on all the coated samples with a load of 1471 N. The area around the indentation were observed with SEM. The results presented in Figure 4.8 has demonstrated that nanodiamond incorporated N-DLC films have enhanced adhesion compared to DLC with nanodiamonds. Figure 4.22 presents the SEM images of the samples with different nitrogen contents after Rockwell C adhesion testing. It can be seen that increase in nitrogen concentration in the coating improves adhesion. With 1 sccm nitrogen flow rate, there is local delamination around the indentation area, little delamination is observed for higher nitrogen flow

rate. As described in section 4.1, pre-deposition of nanodiamond particles on titanium alloy substrate facilitates the formation of titanium carbide, which greatly enhances the interfacial bonding strength. Increased flow rate of nitrogen promotes formation of sp^2 bonded structureas

can be seen from the increasing D of peak in Raman spectra (Figure 4.15). Fitting of the XPS spectra showed similar consistent result about the chemical structure of N-DLCs (Figure 4.19). The decrease in the C-C sp^3 bonding by nitrogen doping with nitrogen coordinated sp^2 structures in the coating probably reduces the strain energy in the coating, thus reducing the internal compressive stress, further enhancing adhesion (Hu et al. 1998). Reduction of stress by nitrogen doping in amorphous carbon structure is well documented by previous researches (Dwivedi et al. 2011; Hu et al. 1998; Kumar et al. 1999). Co-incorporation of nanodiamond and nitrogen further enhances the adhesion of DLC to titanium alloy substrate.

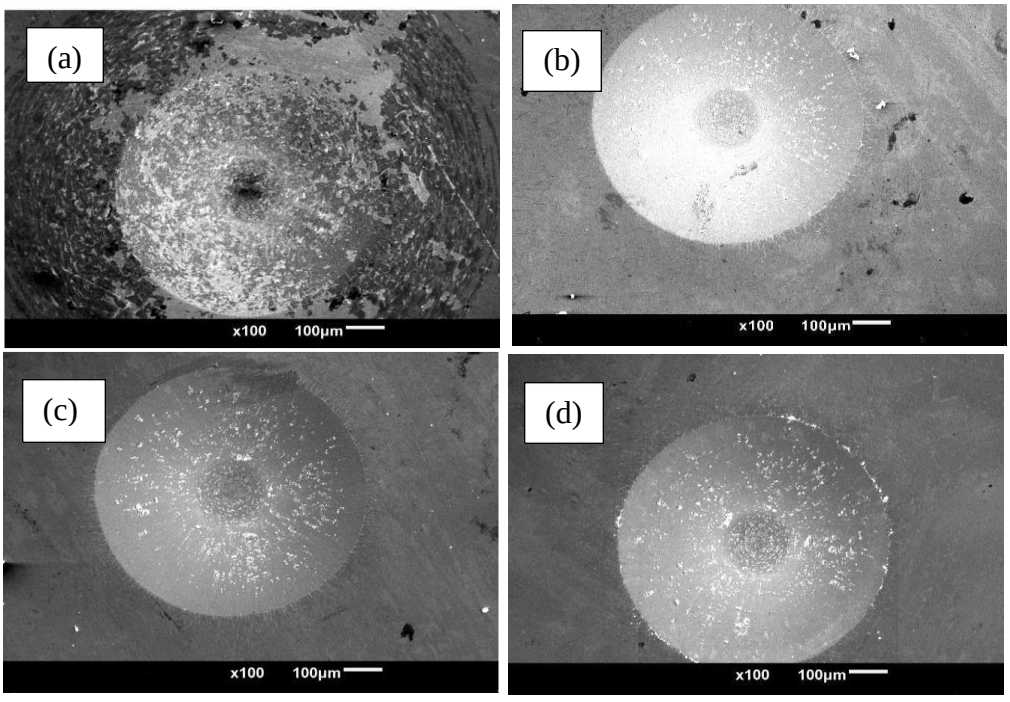

Figure 4.22 SEM images after Rockwell C adhesion testing (a) N-DLC 1 sccm (b) N-DLC 2 sccm, (c) N-DLC 3sccm, (d) N-DLC 6 sccm

4.2.5 Friction and Wear

Friction and wear of ND/N-DLC thin films on titanium alloy substrates were determined using reciprocating ball-on-disk configuration at constant speed of 6mm/sec in ambient conditions. Coefficient of friction (COF) measured against ultra- high molecular polyethylene (UHMPE) balls with 4N load for a period of 1000 cycles showed a decreasing trend with the increase of nitrogen concentration. The samples were numbered for convenience in their respective N/C ratio: Sample 1 as bare titanium alloy substrate; Sample 2 for N/C ratio of 0.24; Sample 3 for N/C ratio of 0.25; Sample 4 for N/C of 0.27 and Sample 5 for N/C of 0.42. The mean steady state friction coefficient

measured on Sample 1 is 0.250 while it decreases to 0.100 for sample 2, 0.098 for sample 3, 0.090 for sample 4 and 0.066 for sample 5. The surface shows no visible wear track against UHMPE balls, indicating little wear.

Coatings tested against 440C stainless steel (AISI 440C) shows slightly higher COF at 1N load. A COF 0.423 is observed on a bare titanium alloy. The COF measured is 0.365, 0.409, 0.267, and 0.179 respectively for sample 2, sample 3,sample 4 and sample 5, respectively, indicating thatthe N-DLC coatings decrease COF of titanium alloy substrates against steel balls and the higher the Nitrogen content, the lower the COF. The width of the wear tracks shows significant decrease for coated titanium alloys compared to bare titanium substrate alloy, as shown in Figure 4.23. Sample 4 with N/C ratio of 0.27 shows the least wear track width and wear rate. The variation of COF against UHMPE and stainless steel 440C balls for various N/C ratio are illustrated in Figure 4.24. The wear rate of the coatings were evaluated by calculating the worn volume per sliding distance per load and listed in Table 4.4. It can be seen that the wear rate is significantly reduced on coated titanium alloys.

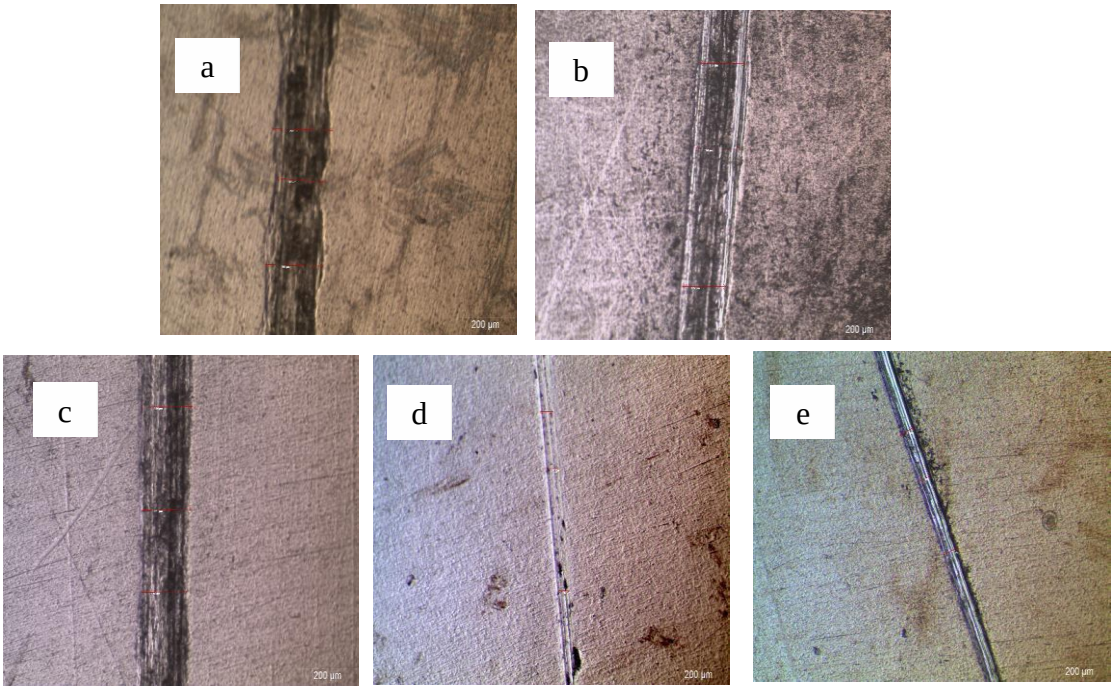

Figure 4.23 Wear track on N-DLC coatings against AISI440C stainless steel balls (a) Sample 1, (b) Sample2, (c) Sample 3, (d) Sample 4, and (e) Sample 5

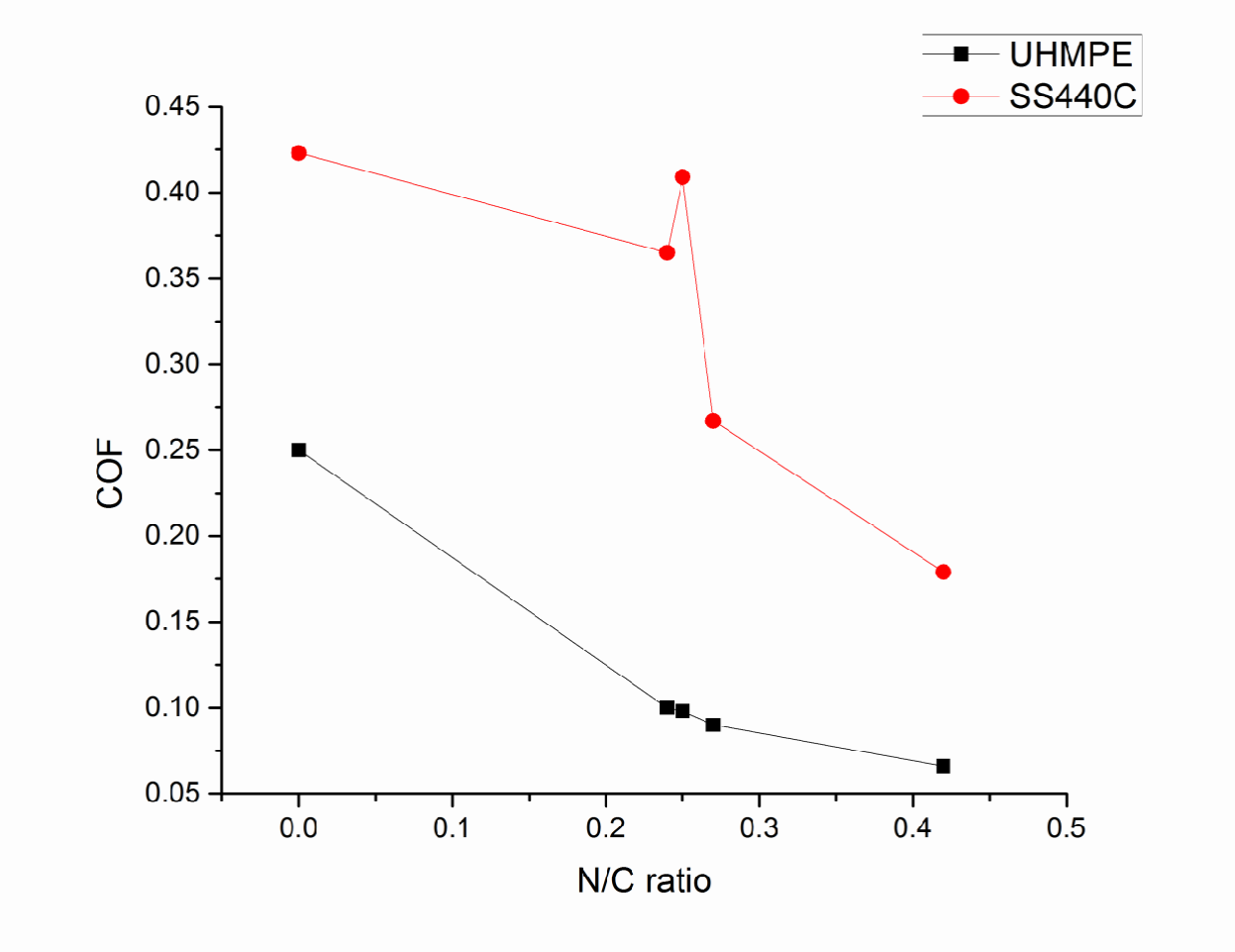

Figure 4.24 COF (coefficient of friction) against UHMPE and AISI440C balls versus N/C (nitrogen to carbon) ratio

Table 4.4 Wear rate data for ND/N-DLC coatings against SS 440C balls

Samples	Average wear rates (x 10^{-9} mm^3 N^{-1} m^{-1})
Sample 1	383.0 ± 5.4
Sample 2	147.0 ± 5.0
Sample 3	144.0 ± 4.6
Sample 4	1.2 ± 0.2
Sample 5	1.5 ± 0.2

The tribological properties of DLC based coatings depend on several factors such as hardness, roughness, bonding structure, relative humidity, temperature, and adhesion to the substrate (Mahmud et al. 2014). The decrease of COF with increase in nitrogen content in films could be attributed to the increase in N/C ratio in the coating which promotes graphitic phases as revealed by Raman and XPS. The easy shear of sp^2 bonded graphitic planes accounts for low COF (Fontaine et al. 2008). The reduced wear rate of coated samples is probably due to the enhanced hardness and reduced COF of coated surface. The effect of nitrogen content on wear rate of ND/N-DLC coated samples is more complicated and can be explained by combining a few factors. When the nitrogen content in the film is low, the C=N/C-C ratio is relatively low, and thus high intrinsic stress still remains in the coating, which causes poor adhesion and delamination from the substrate during wear cycles (Deng & Braun, 1995). And the higher the nitrogen concentration, the lower the stress, and thus the lower the wear rate. With a relatively high nitrogen concentration, the stress would be low enough to prevent delamination. In this case, further increase nitrogen content would increase wear rate because of the reduced hardness induced by the higher content of nitrogen (Holmberg et al. 2007). For the samples tested with UHMWPE balls, the lack of wear of DLC was due to the low hardness of UHMWPE compared to DLC coatings. In this case, only UHMWPE is worn off. The results do not show correlations between COF and wear rate, this is probably due to the large hardness difference between DLC and UHMWPE balls.

4.2.6Electrochemical Impedance Spectroscopy

Figure 4.25 presents the electrochemical impedance plots and Bode phase plots of ND-N-DLC coated Ti alloy. Those plots represent the response to Bode impedance and phase shifts of the ND/N-DLC coated samples in 0.89% NaCl solution for a frequency range of 100 kHz to 10 mHz. The impedance plots give information about the corrosion resistance of the coatings. The impedance at the higher frequencies generally gives information about the resistance of the electrolytes while the impedance at the low frequencies gives information about the protective efficiency of the coatings (Lasia, 1999). The Bode plots comprise two distinct regions, a region of high frequency and a region of low frequency. In the high frequency region from 1 kHz to 100 kHz the Bode impedance plot is parallel to the x-axis, which is logarithmic frequency and has a phase angle of 0^0. This is the region showing response to the solution or electrolytic resistance (R_s). In the middle frequency to the low frequency region the slope of the log |Z| vs log (frequency) the spectra displays a slope of -1 which gradually decreases while the phase angle plot gradually approaches the phase difference of -90^0. This shows that the coatings exhibited some characteristic capacitive behavior as shown in Figure 4.25(b). Similar capacitive response by bare titanium is mainly due to its tendency to form passive oxide (González & Mirza-Rosca, 1999). An ideal coating behaves as a pure capacitor by hindering charge flow, however in practical situations, most of the coatings have defects, areas of low crosslinking and inhomogeneity. Thus coatings in applications rarely behave as a true capacitor (Lasia, 1999). Constant Phase Elements (CPE) are mostly used to replace the true capacitance in real electrolytic solutions. Its impedance is defined by:

$$(CPE) = \frac{1}{[(j\omega)^{n}]} \qquad (4.2)$$

where Y is the admittance of the CPE, w being the angular frequency whereas the exponent 'n' determines the nature of constant phase element. Admittance (Y) is a measure of the fact how easily a current will flow in an electrical circuit. It is generally defined by reciprocal of impedance.

The CPE acts as a pure resistor for n=0, as capacitor for n=1 and behaves as inductor for n= -1

(Azzi et al. 2009; Liu et al. 2001). However in the present work, value of 'n' was close to 1 which signifies capacitive characteristics of the coating at the interface. Comprehensive understanding of the protective efficiency of the coating can be obtained by fitting a model according to the nature of bode impedance plot and phase plot. Numerous models have been suggested to effectively explain the characteristics of the coated surface in electrolyte using EIS techniques (Lasia, 1999). At higher frequencies the phase shift is close to -10^0 for both coated and bare titanium alloys, which shows ohmic behavior dominating the impedance contributed by the solution/electrolytic resistance. At lower frequencies for the ND/N-DLC coated samples the phase shift approaches to -70^0, representing capacitive behavior of the coatings. The plots of the coated samples and bare sample were characterized with two time constant model as shown in Figure 4.26.

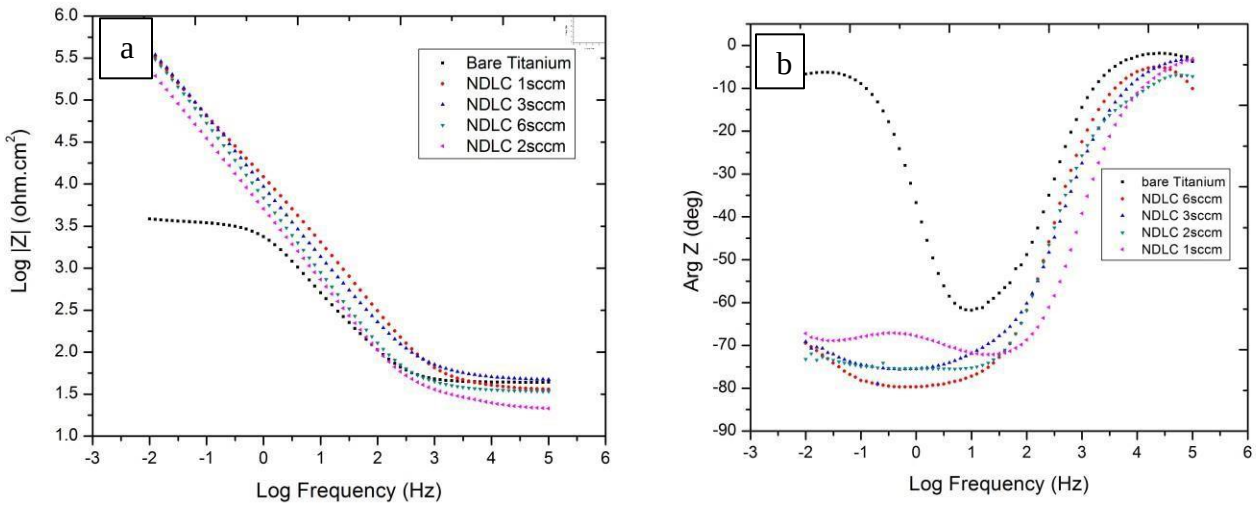

Figure 4.25 (a) Electrochemical Impedance Plot, and (b) Bode Phase Plots of ND-N-DLC coated Ti alloys

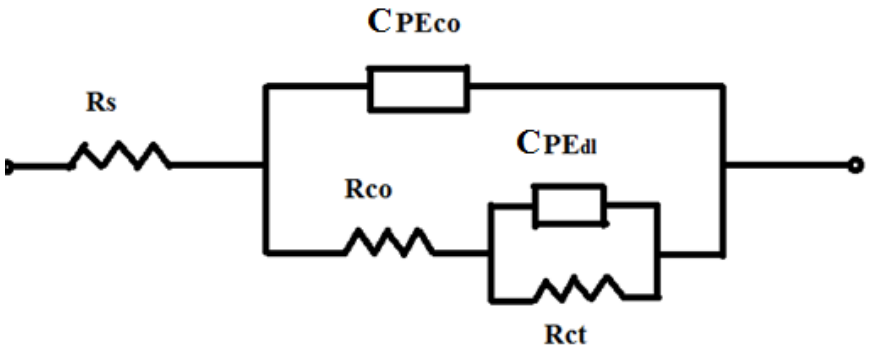

Figure 4.26 Equivalent circuits with two constant phase elements used for EIS spectra

where R_S stands for electrolytic resistance, R_{co} stands for coating resistance (pore resistance) and constant phase element, CPE_{co}, or non-ideal capacitance of the coating. The other resistance, R_{ct} stands for the charge transfer resistance between the solution and the substrate while CPE_{dl} represents double layer capacitance. The values of R_{co} and CPE_{co} is greatly dependent on the total area of the substrate covered by the coating, thickness of the coating, defects in the coating such as stress points and pin holes and microstructural property of the coating such as chemical bonding (Liu et al. 1999).

Table 4.5 The data derived from EIS plots fitting with equivalent model

Sample	Rs	CPE_{co}	α	R_{co}	CPE_{dl}	β	R_{ct}
Bare	43.4	63.3×10^{-6}	0.8	0.3×10^{3}	38.9×10^{-3}	0.7	2.6×10^{3}
N-DLC 1sccm	37.6	14.7×10^{-6}	0.8	24.8×10^{3}	7.7×10^{-6}	0.8	4.5×10^{6}
N-DLC 2sccm	25.1	42.8×10^{-6}	0.8	1.7×10^{3}	6.0×10^{-6}	0.8	1.8×10^{6}
N-DLC 3sccm	44.6	7.6×10^{-6}	0.8	4.3×10^{3}	14.4×10^{-6}	0.8	3.1×10^{6}
N-DLC 6sccm	34.4	2.9×10^{-6}	0.9	1.8×10^{5}	5.9×10^{-6}	0.8	7.8×10^{6}

R_s = Solution resistance measured in ohm.cm^2

CPE_{co} = Constant Phase Element for of the coating measured in F/cm^2

R_{CO} = Resistance offered by the coating measured in ohm.cm^2

CPE_{DL} = Constant Phase element of the double layer measured in F/cm^2

R_{CT} = Charge transfer resistance between the substrate and solution in ohm.cm^2

α , β are constants which shows deviance of the coatings and double layer from pure capacitance behavior in practical conditions.

For our present investigation, a two time constant model was assumed also for the bare titanium alloy because titanium alloy has a tendency to form titanium oxide layers on its surface (González & Mirza-Rosca, 1999). R_{co} gives the coating characteristics and reflects the degree to which a film

forms a barrier to the electrolytic conduction. Penetration of the electrolyte or solution can occur through microscopic pores, areas of defect or low cross-linking (Maguire et al. 2005).On bare titanium alloy this resistance signifies the resistance of the passive oxide film. ND/N-DLC coated substrates showed an increase in R_{co} values. DLC doped with 6sccm nitrogen showed the highest coating resistance. Even though I_D/I_G ratio is highest for coating prepared with 6 sccm nitrogen flow rate indicating high amount of sp^2 bonding but its high corrosion resistance is attributed greatly to its lower stress and thus lesser defect pathways for electrolyte as nitrogen doping can greatly reduce the stress in coating (Hu et al. 1998). Charge transfer resistance, $R_{ct,}$ relates to the bare titanium alloy shows 2.6 x 10^3 ohms which increases by three orders of magnitude with ND/N-DLC coating. Corrosion resistance provided by the titanium oxide layer to bare titanium alloys can greatly be enhanced by the well adherent carbon coatings as shown in Table 4.5. Figure 4.27 shows the schematic diagram of coating defects

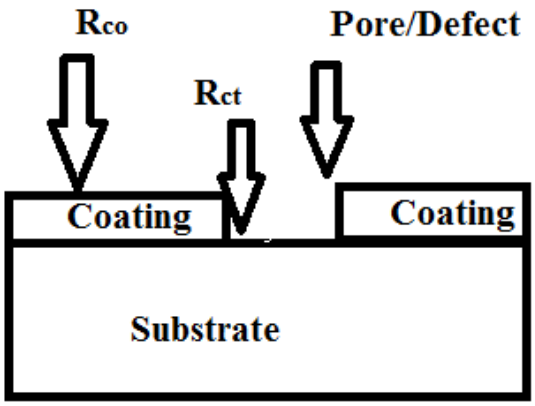

Figure 4.27 Schematic diagram showing of coating defects (pore), charge transfer resistance Rct and Coating resistance Rco

Chapter 5

Conclusions and Recommended Future Work

5.1 Summary and Conclusions

Adhesive, mechanical, tribological and electrochemical properties of DLC and N-DLCs on titanium alloys deposited by ion beam deposition were investigated by various advanced techniques. The conclusions are summarized as follows:

1. DLC deposited on bare titanium alloy shows premature delamination by buckling. nanodiamond and nitrogen incorporation can greatly enhance the adhesion of the coating to the titanium alloy substrate.
2. Adhesion can be further improved by increasing nitrogen doping concentration.
3. Nitrogen doping decreases roughness and hardness of DLC films. The higher the nitrogen content, the lower the roughness and the hardness.
4. DLC coatings slide against SS 440C balls and UHMWPE balls in ambient atmosphere with 40% relative humidity shows that DLC based coatings decrease COF and the higher the nitrogen content, the lower the COF. No visible wear were observed on the coatings when sliding against UHMWPE balls. Coatings shows increased wear resistance (lower wear rate) against AISI 440C balls compared to the bare titanium alloys. ND/N-DLC coating prepared with 3sccm nitrogen flow rate shows the lowest wear rate (highest wear resistance) because of the low stress, high adhesion and relatively high hardness.
5. Due to excellent adhesion and lowered stress, ND/N-DLC coatings greatly enhances the corrosion resistance of the titanium alloy as demonstrated by linear polarization tests and electrochemical impedance spectroscopic tests.

5.2 Recommended future work

The nanodiamond incorporated N-DLC coatings show promising mechanical, tribological, and corrosion resistant properties, it would be desirable do more systematic research to optimize the

coating structure (thickness, nitrogen content, nanodiamond distribution and concentration, bonding states etc) to achieve optimized properties (high density, high adhesion, low stress, high hardness etc) for their practical application. As a potential coating for biomedical applications, its corrosion resistance in solutions with different pH values and simulated body fluids should be tested along with simulated testing of tribological properties in a corrosive environment.

List of References:

Agins, H. J., Alcock, N. W., Bansal, M., Salvati, E. A, Wilson, P. D., Pellicci, P. M., & Bullough, P. G. (1988). Metallic wear in failed titanium-alloy total hip replacements. A histological and quantitative analysis. The Journal of Bone and Joint Surgery. American Volume, 70, 347–56. doi:10.5772/1928

Aisenberg, S., & Chabot, R. (1971). Ion-beam deposition of thin films of diamondlike carbon. Journal of Applied Physics, 42(1971), 2953–2958. doi:10.1063/1.1660654

Al Mahmud, K. a. H., Kalam, M. a., Masjuki, H. H., Mobarak, H. M., & Zulkifli, N. W. M. (2014). An updated overview of diamond-like carbon coating in tribology. Critical Reviews in Solid State and Materials Sciences, 40(November), 90–118. doi:10.1080/10408436.2014.940441

Anita, V., Butuda, T., Maeda, T., Takizawa, K., Saito, N., & Takai, O. (2004). Effect of N doping on properties of diamond-like carbon thin films produced by RF capacitively coupled chemical vapor deposition from different precursors. Diamond and Related Materials, 13, 1993–1996. doi:10.1016/j.diamond.2004.05.002

Azzi, M., Paquette, M., Szpunar, J. A., Klemberg-Sapieha, J. E., & Martinu, L. (2009). Tribocorrosion behaviour of DLC-coated 316L stainless steel. Wear, 267, 860–866. doi:10.1016/j.wear.2009.02.006

Berkeley, L. (2001). Lawrence Berkeley National Laboratory Synthesis, properties and applications of pure and covalently doped DLC films prepared by energetic condensation.

Bilek, M. M. M., & McKenzie, D. R. (2006). A comprehensive model of stress generation and relief processes in thin films deposited with energetic ions. Surface and Coatings Technology, 200, 4345–4354. doi:10.1016/j.surfcoat.2005.02.161

Box, P. O., & Scala, I.-M. (1995). Related materials, 4, 1–4.

Boyer, R. R. (1996). An overview on the use of titanium in the aerospace industry. Materials Science and Engineering A, 213, 103–114. doi:10.1016/0921-5093(96)10233-1

Budinski, K. G. (1991). Tribological properties of titanium-alloys. Wear, 151, 203–217. doi:10.1016/0043-1648(91)90249-T

Casiraghi, C., Ferrari, A.C., & Robertson, J. (2005). Raman spectroscopy of hydrogenated amorphous carbons. Physical Review B - Condensed Matter and Materials Physics, 72(August), 1–14. doi:10.1103/PhysRevB.72.085401

Casiraghi, C., Piazza, F., Ferrari, a. C., Grambole, D., & Robertson, J. (2005). Bonding in hydrogenated diamond-like carbon by Raman spectroscopy. Diamond and Related Materials, 14, 1098–1102. doi:10.1016/j.diamond.2004.10.030

Chang, C. L., & Wang, D. Y. (2001). Microstructure and adhesion characteristics of diamond-like carbon films deposited on steel substrates. Diamond and Related Materials, 10, 1528–1534. doi:10.1016/S0925-9635(01)00382-X

Cheah, L. K., Shi, X., Shi, J. R., Liu, E. J., & Silva, S. R. P. (1998). Properties of nitrogen doped tetrahedral amorphous carbon films prepared by filtered cathodic vacuum arc technique. Journal of Non-Crystalline Solids, 242, 40–48. doi:10.1016/S0022-3093(98)00787-X

Choy, K.-L., & Felix, E. (2000). Functionally graded diamond-like carbon coatings on metallic substrates. Materials Science and Engineering: A, 278, 162–169. doi:10.1016/S0921-5093(99)00569-9

Costa, M. Y. P., Venditti, M. L. R., Cioffi, M. O. H., Voorwald, H. J. C., Guimarães, V. a., & Ruas, R. (2011). Fatigue behavior of PVD coated Ti-6Al-4V alloy. International Journal of Fatigue, 33, 759–765. doi:10.1016/j.ijfatigue.2010.11.007

Das, D., Chen, K. H., Chattopadhyay, S., & Chen, L. C. (2002). Spectroscopic studies of nitrogenated amorphous carbon films prepared by ion beam sputtering. Journal of Applied Physics, 91, 4944–4955. doi:10.1063/1.1459610

Deng, J., & Braun, M. (1995). DLC multilayer coatings for wear protection. Diamond and Related Materials, 4(94), 936–943. doi:10.1016/0925-9635(94)00256-8

Donnet, C. (1998). Recent progress on the tribology of doped diamond-like and carbon alloy coatings: a review. Surface and Coatings Technology, 100-101, 180–186. doi:10.1016/S0257-8972(97)00611-7

Dwivedi, N., Kumar, S., Rauthan, C. M. S., & Panwar, O. S. (2011). Nano indentation measurements on nitrogen incorporated diamond-like carbon coatings. Applied Physics A: Materials Science and Processing, 102, 225–230. doi:10.1007/s00339-010-5908-5

Erdemir, A., & Donnet, C. (2006). Tribology of diamond-like carbon films: recent progress and future prospects. Journal of Physics D: Applied Physics, 39, R311–R327. doi:10.1088/0022-3727/39/18/R01

Fasel, R., Aebi, P., Schlapbach, L., Greber, T., & Osterwalder, J. (1997). Electronic and Atomic Structure of. Surface Review and Letters, 04, 1155–1160. doi:10.1142/S0218625X97001462

Ferrari, A. C., Rodil, S. E., & Robertson, J. (2003). Interpretation of infrared and Raman spectra of amorphous carbon nitrides. Physical Review B, 67, 155306. doi:10.1103/PhysRevB.67.155306

Fontaine, J., Donnet, C., & Erdemir, a. (2008). Tribology of Diamond-Like Carbon Films (p. 140). doi:10.1007/978-0-387-49891-1

González, J. E. . E. G., & Mirza-Rosca, J. . C. (1999). Study of the corrosion behavior of titanium and some of its alloys for biomedical and dental implant applications. Journal of Electroanalytical Chemistry, 471, 109–115. doi:10.1016/S0022-0728(99)00260-0

Graner, F., & Glazier, J. A. (1992). Ph Ysical Review. Physical Review Letters, 69(8), 2013–2016. doi:10.1103/PhysRevLett.70.694

Grill, A. (1993). Review of the tribology of diamond-like carbon. Wear, 168, 143–153. doi:10.1016/0043-1648(93)90210-D

Grill, A. (1997). Tribology of diamondlike carbon and related materials: an updated review. Surface and Coatings Technology, 94-95, 507–513. doi:10.1016/S0257-8972(97)00458-1

Grill, A. (2003). Diamond-like carbon coatings as biocompatible materials—an overview. Diamond and Related Materials, 12, 166–170. doi:10.1016/S0925-9635(03)00018-9

Hayashi, Y., Krishna, K. M., Ebisu, H., Soga, T., Umeno, M., & Jimbo, T. (2001). Optical and structural properties of nitrogen doped amorphous carbon films grown by rf plasma-enhanced CVD, 1002–1006.

Heinke, W., Leyland, A., Matthews, A., Berg, G., Friedrich, C., & Broszeit, E. (1995). Evaluation of PVD nitride coatings, using impact, scratch and Rockwell-C adhesion tests. Thin Solid Films, 270, 431–438. doi:10.1016/0040-6090(95)06934-8

Holmberg, K., Ronkainen, H., Laukkanen, A., & Wallin, K. (2007). Friction and wear of coated surfaces — scales, modelling and simulation of tribomechanisms. Surface and Coatings Technology, 202, 1034–1049. doi:10.1016/j.surfcoat.2007.07.105

Hu, J., Yang, P., & Lieber, C. M. (1998). Nitrogen-driven sp 3 to sp 2 transformation in carbon nitride materials, 57(6), 3185–3188.

Kim, H. G., Ahn, S. H., Kim, J. G., Park, S. J., & Lee, K. R. (2005). Corrosion performance of diamond-like carbon (DLC)-coated Ti alloy in the simulated body fluid environment. Diamond and Related Materials, 14, 35–41. doi:10.1016/j.diamond.2004.06.034

Kumar, S., Dixit, P. N., Sarangi, D., & Bhattacharyya, R. (1999). Possible solution to the problem of high built-up stresses in diamond-like carbon films. Journal of Applied Physics, 85(1999), 3866. doi:10.1063/1.369758

Lasia, A. A. (1999). Electrochemical Impedance Spectroscopy and its Applications. Electrochemical Impedance Spectroscopy and Its Applications, Modern Aspects of Electrochemistry (Vol. 32, pp. 143–248). doi:10.1007/978-1-4614-8933-7

Lettington, A. H. (1998). Applications of diamond-like carbon thin films. Carbon, 36(556), 555–560. doi:10.1016/S0008-6223(98)00062-1

Lifshitz, Y. (1999). Diamond-like carbon — present status. Diamond and Related Materials, 8(8-9), 1659–1676. doi:10.1016/S0925-9635(99)00087-4

Liu, C., Bi, Q., & Matthews, A. (2001). EIS comparison on corrosion performance of PVD TiN and CrN coated mild steel in 0.5 N NaCl aqueous solution. Corrosion Science, 43, 1953–1961. doi:10.1016/S0010-938X(00)00188-8

Liu, Z. H., Zhao, J. F., & McLaughlin, J. (1999). A study of microstructural and electrochemical properties of ultra-thin DLC coatings on altic substrates deposited using the ion beam technique. Diamond and Related Materials, 8, 56–63. doi:10.1016/S0925-9635(98)00364-1

Ma, G., Gong, S., Lin, G., Zhang, L., & Sun, G. (2012). A study of structure and properties of Ti-doped DLC film by reactive magnetron sputtering with ion implantation. Applied Surface Science, 258(7), 3045–3050. doi:10.1016/j.apsusc.2011.11.034

Ma, K., Yang, G., Yu, L., & Zhang, P. (2010). Synthesis and characterization of nickel-doped diamond-like carbon film electrodeposited at a low voltage. Surface and Coatings Technology, 204(16-17), 2546–2550. doi:10.1016/j.surfcoat.2010.01.039

Maguire, P. D., McLaughlin, J. A, Okpalugo, T. I. T., Lemoine, P., Papakonstantinou, P., McAdams, E. T., Abbas, G. A (2005). Mechanical stability, corrosion performance and bioresponse of amorphous diamond-like carbon for medical stents and guidewires. Diamond and Related Materials, 14, 1277–1288. doi:10.1016/j.diamond.2004.12.023

Marton, M., Kovalčík, D., Vojs, M., Zdravecká, E., Varga, M., Michalíková, L., … Písečný, P. (2012). Electrochemical corrosion behavior of amorphous carbon nitride thin films. Vacuum, 86, 696–698. doi:10.1016/j.vacuum.2011.07.053

McCann, R., Roy, S. S., Papakonstantinou, P., Bain, M. F., Gamble, H. S., & McLaughlin, J. a. (2005a). Chemical bonding modifications of tetrahedral amorphous carbon and nitrogenated tetrahedral amorphous carbon films induced by rapid thermal annealing. Thin Solid Films, 482, 34–40. doi:10.1016/j.tsf.2004.11.151

McCann, R., Roy, S. S., Papakonstantinou, P., Bain, M. F., Gamble, H. S., & McLaughlin, J. a. (2005b). Chemical bonding modifications of tetrahedral amorphous carbon and nitrogenated tetrahedral amorphous carbon films induced by rapid thermal annealing. Thin Solid Films, 482, 34–40. doi:10.1016/j.tsf.2004.11.151

Mosaner, P., Bonelli, M., & Miotello, A. (2003). Pulsed laser deposition of diamond-like carbon films: Reducing internal stress by thermal annealing. Applied Surface Science, 208-209, 561–565. doi:10.1016/S0169-4332(02)01383-1

Oliver, W. C., & Pharr, G. M. (1992). experiments.

Pauleau, Y. (2001). Generation and evolution of residual stresses in physical vapour-deposited thin films. Vacuum, 61, 175–181. doi:10.1016/S0042-207X(00)00475-9

Peng, X. L., & Clyne, T. W. (1998). Residual stress and debonding of DLC films on metallic substrates. Diamond and Related Materials, 7, 944–950. doi:10.1016/S0925-9635(97)00331-2

Rack, H. J., & Qazi, J. I. (2006). Titanium alloys for biomedical applications. Materials Science and Engineering C, 26, 1269–1277. doi:10.1016/j.msec.2005.08.032

Ray, S. C., Tsai, H. M., Chiou, J. W., Bose, B., Jan, J. C., Kumar, K., … Tsai, M.-H. (2004). X-ray absorption spectroscopy (XAS) study of dip deposited a-C:H(OH) thin films. Journal of Physics: Condensed Matter, 16, 5713–5719. doi:10.1088/0953-8984/16/32/008

Robertson, J. (2002). Diamond-like amorphous carbon. Materials Science and Engineering: R: Reports, 37, 129–281. doi:10.1016/S0927-796X(02)00005-0

Robertson, J. (2005). Mechanism of sp3 bond formation in the growth of diamond-like carbon. Diamond and Related Materials, 14, 942–948. doi:10.1016/j.diamond.2004.11.028

Robertson, J. (2008). Comparison of diamond-like carbon to diamond for applications. Physica Status Solidi (A) Applications and Materials Science, 205(9), 2233–2244. doi:10.1002/pssa.200879720

Roy, R. K., & Lee, K.-R. (2007). Biomedical applications of diamond-like carbon coatings: a review. Journal of Biomedical Materials Research. Part B, Applied Biomaterials, 83(1), 72–84. doi:10.1002/jbm.b.30768

Roy, S. S., McCann, R., Papakonstantinou, P., Maguire, P., & McLaughlin, J. A. (2005). The structure of amorphous carbon nitride films using a combined study of NEXAFS, XPS and Raman spectroscopies. Thin Solid Films, 482, 145–150. doi:10.1016/j.tsf.2004.11.132

Ruijun, Z., & Hongtao, M. (2006). Nano-mechanical properties and nano-tribological behaviors of nitrogen-doped diamond-like carbon (DLC) coatings. Journal of Materials Science, 41(Dlc), 1705–1709. doi:10.1007/s10853-006-2874-6

Sánchez-López, J. C., & Fernández, A. (2008). Doping and alloying effects on DLC coatings. Tribology of Diamond-Like Carbon Films: Fundamentals and Applications, (Dlc), 311–328. doi:10.1007/978-0-387-49891-1_12

Scharf, T. W., Ott, R. D., Yang, D., & Barnard, J. A. (1999). Structural and tribological characterization of protective amorphous diamond-like carbon and amorphous CN[sub x] overcoats for next generation hard disks. Journal of Applied Physics, 85(1999), 3142. doi:10.1063/1.369654

Seker, Z., Ozdamar, H., Esen, M., Esen, R., & Kavak, H. (2014). The effect of nitrogen incorporation in DLC films deposited by ECR Microwave Plasma CVD. Applied Surface Science, 314, 46–51. doi:10.1016/j.apsusc.2014.06.137

Singh, V., Palshin, V., Tittsworth, R. C., & Meletis, E. I. (2006). Local structure of composite Cr-containing diamond-like carbon thin films. Carbon, 44, 1280–1286. doi:10.1016/j.carbon.2005.10.048

Srinivasan, S., Tang, Y., Li, Y. S., Yang, Q., & Hirose, A. (2012). Ion beam deposition of DLC and nitrogen doped DLC thin films for enhanced haemocompatibility on PTFE. Applied Surface Science, 258, 8094–8099. doi:10.1016/j.apsusc.2012.04.178

Sullivan, J. P., Friedmann, T. A, & Baca, A. (1997). Stress Relaxation and Thermal Evolution of Film Properties in Amorphous Carbon. Journal of Electronic Materials, 26(9).

Tang, Y. H., Zhang, P., Kim, P. S., Sham, T. K., Hu, Y. F., Sun, X. H., Lee, S. T. (2001). Amorphous carbon nanowires investigated by near-edge-x-ray-absorption-fine-structures. Applied Physics Letters, 79(2001), 3773–3775. doi:10.1063/1.142

Tang, Y., Li, Y. S., Yang, Q., & Hirose, A. (2011). Characterization of hydrogenated amorphous carbon thin films by end-Hall ion beam deposition. Applied Surface Science, 257, 4699–4705. doi:10.1016/j.apsusc.2010.12.129

Voevodin, A. A., O'Neill, J. P., & Zabinski, J. S. (1999). Nanocomposite tribological coatings for aerospace applications. Surface and Coatings Technology, 116-119, 36–45. doi:10.1016/S0257-8972(99)00228-5

Wei, C., Wang, Y. S., & Tai, F. C. (2009). The role of metal interlayer on thermal stress, film structure, wettability and hydrogen content for diamond like carbon films on different substrate. Diamond and Related Materials, 18(2-3), 407–412. doi:10.1016/j.diamond.2008.11.009

Wu, G., Sun, L., Dai, W., Song, L., & Wang, A. (2010). Influence of interlayers on corrosion resistance of diamond-like carbon coating on magnesium alloy. Surface and Coatings Technology, 204(14), 2193–2196. doi:10.1016/j.surfcoat.2009.12.009

Wu, W.-J., Pai, T.-M., & Hon, M.-H. (1998). Wear behavior of silicon-containing diamond-like carbon coatings. Diamond and Related Materials, 7(June), 1478–1484. doi:10.1016/S0925-9635(98)00213-1

Xps, T. (2013). XPS Spectra. *, 1–77

Yamada, M. (1996). An overview on the development of titanium alloys for non-aerospace application in Japan. Materials Science and Engineering A, 213, 8–15. doi:10.1016/0921-5093(96)10241-0

Zhang, C. Z., Tang, Y., Li, Y. S., & Yang, Q. (2013). Adhesion enhancement of diamond-like carbon thin films on Ti alloys by incorporation of nanodiamond particles. Thin Solid Films, 528, 111–115. doi:10.1016/j.tsf.2012.05.094

Zhang, L., & Koka, R. V. (1998). A study on the oxidation and carbon diffusion of TiC in alumina–titanium carbide ceramics using XPS and Raman spectroscopy. Materials Chemistry and Physics, 57, 23–32. doi:10.1016/S0254-0584(98)00187-4

Zhang Linlin. (2012). Synthesis and Characterization of Boron Incorporated Diamond-Like Carbon Thin Films

Zhou, K., Ke, P., Li, X., Zou, Y., & Wang, A. (2015). Microstructure and electrochemical properties of nitrogen-doped DLC films deposited by PECVD technique. Applied Surface Science, 329, 281–286. doi:10.1016/j.apsusc.2014.12.162

Zou, Y. S., Wang, Q. M., Du, H., Song, G. H., Xiao, J. Q., Gong, J., Wen, L. S. (2005). Structural characterization of nitrogen doped diamond-like carbon films deposited by arc ion plating. Applied Surface Science, 241(3-4), 295–302. doi:10.1016/j.apsusc.2004.07.043

Zou, Y. S., Wu, Y. F., Huang, R. F., Sun, C., & Wen, L. S. (2009). Mechanical properties and thermal stability of nitrogen incorporated diamond-like carbon films. Vacuum, 83, 1406–1410. doi:10.1016/j.vacuum.2009.04.072